Development of a Physics-Based Weight (PBWeight) Prediction Tool for Conceptual Design

Tyler Winter[1], José Márquez[2], and Brent Scheneman[3]
M4 Engineering, Inc., Long Beach, California, 90807

I. Introduction

Many critical challenges currently exist for designing, developing, and analyzing physics-based conceptual aircraft design tools. Often engineers struggle with determining the appropriate levels of fidelity in models or techniques (e.g. reduced order) to be used in the conceptual design phase. One challenge of particular relevance to the current effort is the desire to accurately and efficiently predict weights and loadings for unconventional designs. Unconventional designs are required to break through the common or 'expected' limitations associated with conventional designs. Furthermore, the ability to assess, in a rapid manner, the feasibility of these unconventional designs is crucial to NASA's Environmentally Responsible Aviation (ERA) project as well as many other efforts seeking to develop enabling technologies required to solve a variety of important design problems (high lift-to-drag ratios, community noise, reduced drag, etc.). The Blended Wing Body (BWB) or Hybrid Wing Body (HWB) aircraft, for example, has been researched and analyzed for many years as an unconventional efficient transport configuration.

Approaches for weight prediction in the conceptual design phase typically consist of parametric relations or empirical databases (Refs. 1 and 2). Historical databases work reasonably well when applied to existing or conventional designs, however, they fail to predict accurately the weights and loads associated with unconventional designs (like the BWB). There exists a need to augment existing historical databases with a physics-based methodology/capability for predicting the weights and loads of unconventional designs.

In the current effort, M4 Engineering has developed and evaluated the feasibility of an innovative concept aimed at enhancing previously developed databases with physics-based weight and load estimation relationships for unconventional (and conventional!) conceptual wing and fuselage designs. The main goal for this effort will be to develop a software tool capable of generating weight and load responses for unconventional designs from physics-based simulations. In an effort to minimize risk and expedite development, the PBWeight software utilizes a previously developed tool (RapidFEM) to automatically generate geometry and Finite Element Models (FEMs) of complex built-up structures for rapid concept evaluation and structural optimization. The PBWeight software allows a user to specify conceptual design-level information about wing and fuselage structures, then automatically create FEMs and generate relationships (response surfaces) for weights and loads.

In the following section, a brief description of the demonstration configurations analyzed with the PBWeight software is given. In Section III, an overview on the physics-based weight prediction process will be outlined. In Section IV, the details of the configuration development procedure will be given. In Section V, the example problem descriptions and optimization results will be described in detail for each configuration. Finally, in Section VI, the main objectives of our future work will be given.

II. Selection of Conventional and Unconventional Configurations

The aircraft configurations were selected in collaboration with NASA. For the unconventional configuration, the Low Boom Concept Demonstrator (Low Boom) was selected for being the most relevant application for engineers at NASA. Consequently, the MD-87 was chosen to serve as the conventional configuration due to it being a commercial transport of similar length to the Low Boom.

A. Conventional Demonstration Configuration – MD-87

A three-view schematic of the MD-87 aircraft was obtained from Ref. 3, as shown in Figure 1 (left). Moreover, a weight statement for the MD-80 series was obtained from Ref. 1, and shown in Figure 1 (right).

[1] Manager of Research and Development, 4020 Long Beach Blvd, Long Beach, CA, 90807, Member AIAA
[2] Aerospace Engineer, 4020 Long Beach Blvd, Long Beach, CA, 90807, Member AIAA
[3] Computer Engineer, 4020 Long Beach Blvd, Long Beach, CA, 90807

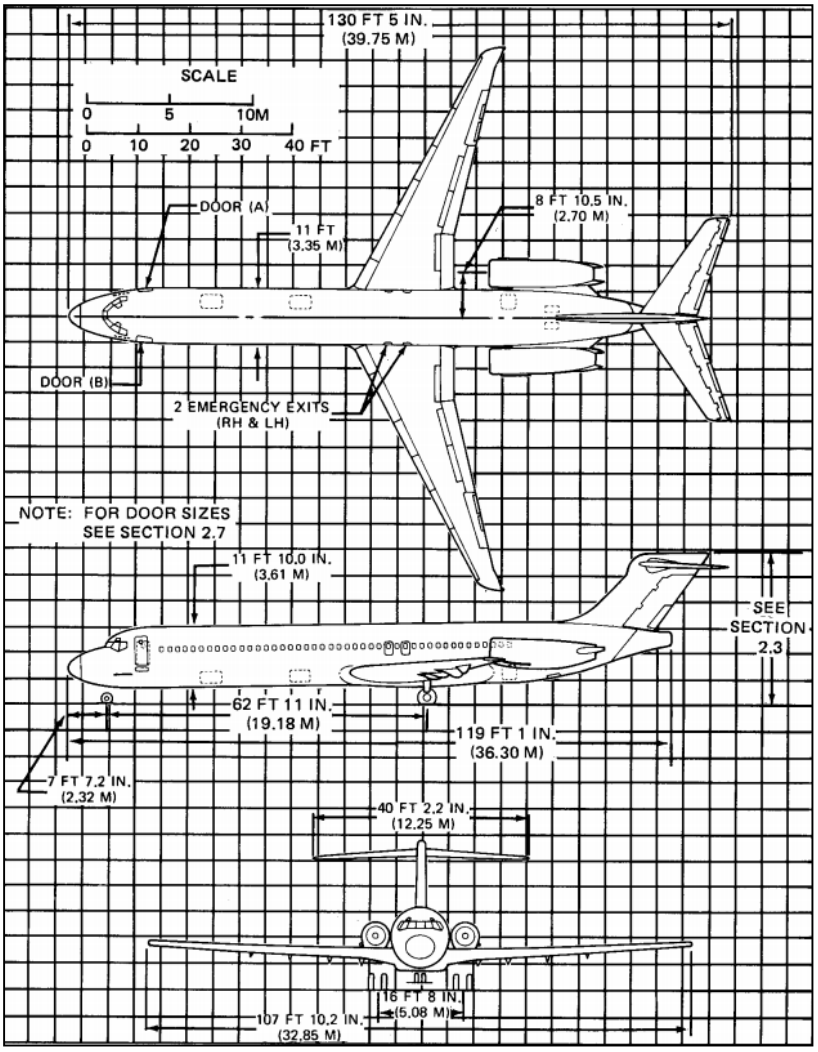

Aircraft	MD-80
Wing	15,560
Empennage	3,320
Fuselage	16,150
Nacelle	5,340
Landing gear	5,340
Nose gear	550
Main gear	4,790
Structure total	42,490
Engine	8,820
Nozzle system and $T_{reverser}$	1,540
Air induction system[a]	0
Fuel system	640
Propulsion install	—
Propulsion total	11,000
Avionics and instruments	2,130
Surface controls	2,540
Hydraulic system	540
Pneumatic system	1,720
Electrical system	—
Electronics	—
Auxiliary power units (APU)	840
Oxygen system	220
Environmental control system (ECS)	1,580
Anti-icing system	550
Furnishings	8,450
Miscellaneous	3,650
Equipment total	25,460
Empty weight (lb)	78,950
Fuel	39,362
Oil	—
Payload (lb)	43,950
TOGW (lb)	140,000
Wing span (ft)	107.7
Wing area, S (ft^2)	1,270
Horizontal tail area, S_H (ft^2)	314
Vertical tail area, S_V (ft^2)	168

[a]Engines in pods, weight included in nacelle.

Figure 1: Three-view Schematic of the MD-87 3 and MD-80 Series Weight Statement (in Pounds) (Ref. 1).

B. Unconventional Demonstration Configuration – Low Boom Concept Demonstrator

A two-view schematic of the Low Boom was obtained from Ref. 4, as shown in Figure 2. Moreover, since the Low Boom is a conceptual vehicle, no official weight statement is currently available. However, for the purpose of comparison, an estimate of the takeoff gross weight (TOGW) was taken from Ref. 4.

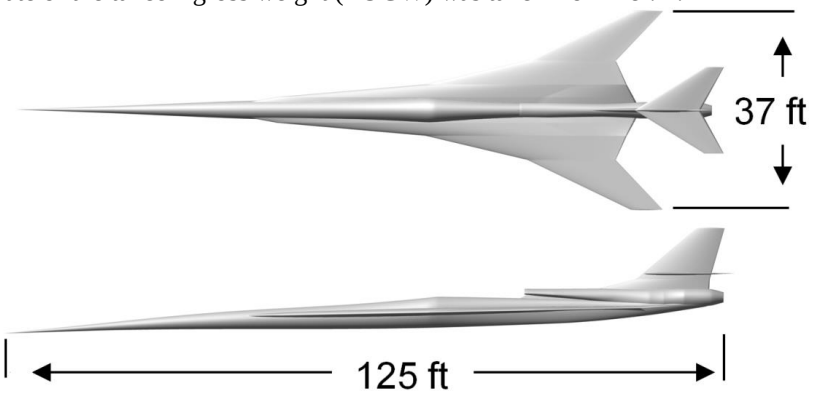

Figure 2: Two-view Schematic of the Low Boom Concept Demonstrator (Ref. 4).

III. Physics-Based Weight Estimation Process

A high-level overview of the process performed by PBWeight is shown in Figure 3. This process includes rapidly creating the parametric geometry definitions, generating suitable Outer Mold Lines (OMLs), developing RapidFEM (Ref. 5) sketch files, and generating/merging the components into finalized FEMs. By utilizing this approach, substantial progress could be made in an efficient manner.

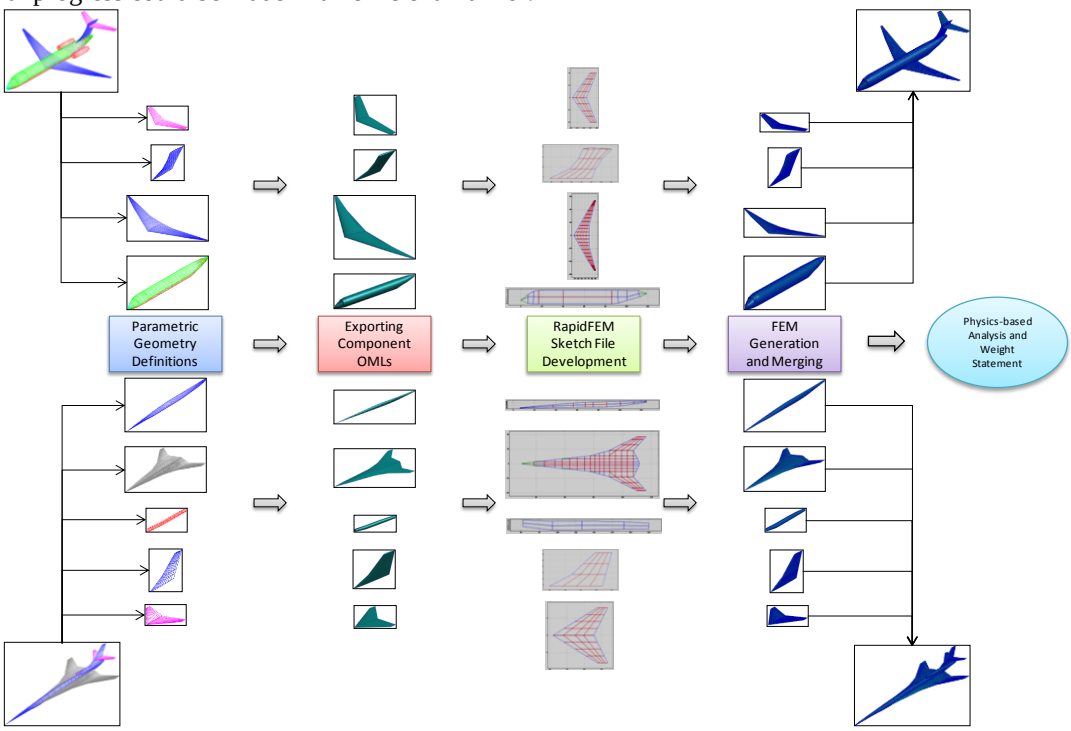

Figure 3: Process Overview for Rapid Parametric FEM Generation.

A. Parametric Geometry Definitions

The first step in the process shown in Figure 3 was to develop parametric geometry representations that resemble each of the configurations. This was accomplished within the Open Vehicle Sketch Pad (OpenVSP) software package, since the accompanying aircraft parameterization style serves as an excellent basis for conceptual-level design and analysis.

The models were then rapidly built within OpenVSP by placing the schematics (i.e. Figure 1 and Figure 2) in the background, fixing component dimensions to published specifications, scaling the components to match the dimensions of the schematic, and shaping the components as necessary. Following this procedure, each model was built within approximately one day of work. Figure 4 through Figure 8 display the overlay comparison between the two OpenVSP models and their corresponding schematics. By observing the overlays, minor discrepancies can be seen. These discrepancies are important for an aerodynamic analysis; however, they become less important when representing an OML to be used in the creation of a structural FEM.

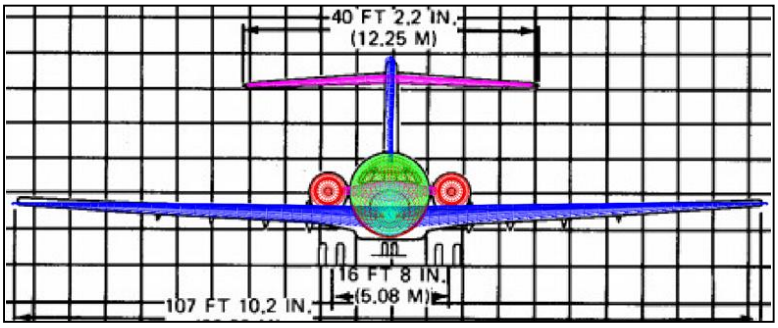

Figure 4: MD-87 Front View.

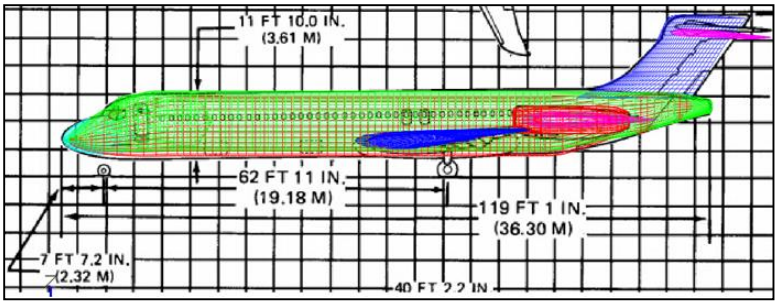

Figure 5: MD-87 Side View.

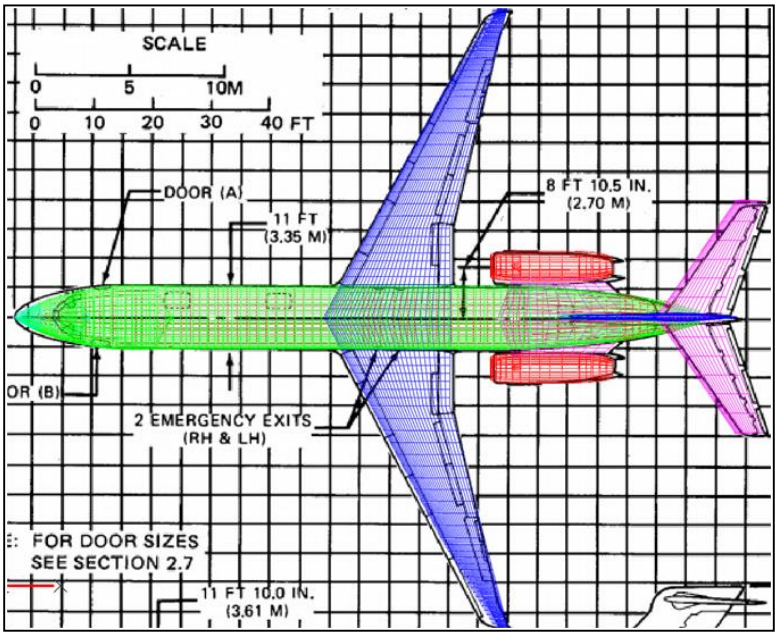

Figure 6: MD-87 Top View.

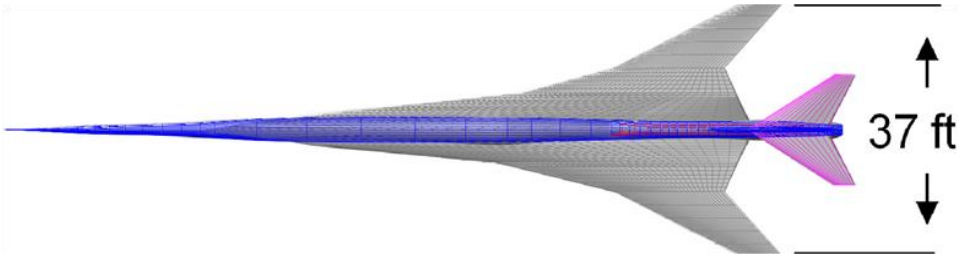

Figure 7: Low Boom Top View.

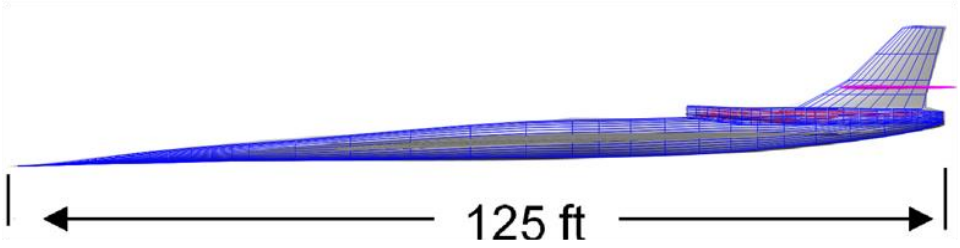

Figure 8: Low Boom Side View.

B. Exporting Component OMLs

The second step in the process shown in Figure 3 was to export a geometric representation (e.g. .step or .iges file format) for each component of each configuration. The OMLs are required by RapidFEM when generating a bounding mesh for the internal structure. Figure 9 and Figure 10 show the MD-87 and Low Boom geometries along with their key component OMLs, respectively.

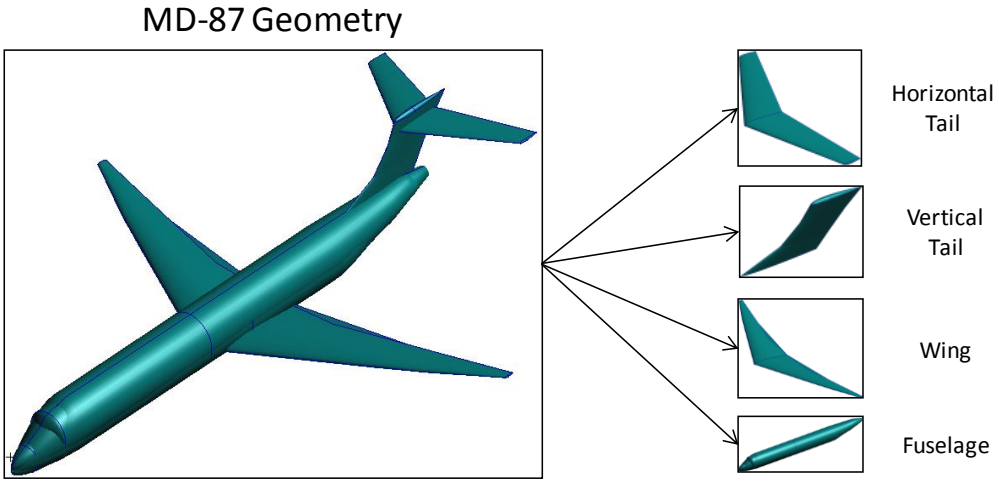

Figure 9: MD-87 Baseline Geometry and Component Geometry OMLs.

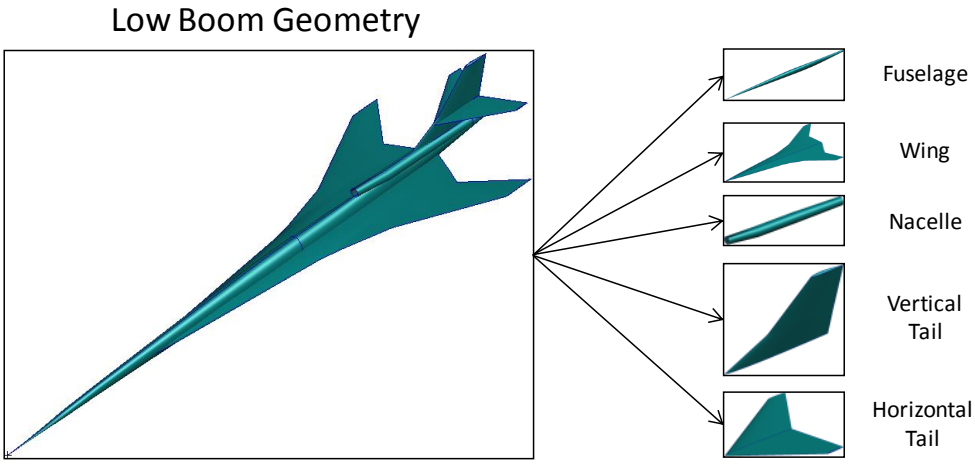

Figure 10: Low Boom Baseline Geometry and Component Geometry OMLs.

C. RapidFEM Sketch File Development

The third step in the process shown in Figure 3 was to create RapidFEM sketch files for each component of each configuration. The sketch file consists of information defining a 2D "sketch," which is projected onto the OML to define the curves and surfaces needed for structural modeling and analysis. Currently this is the most time-intensive task, since it involves defining all necessary details and information regarding the internal structural layout, material property specifications, Non-Structural Mass (NSM) specifications, control surfaces, simulated load cases, and trimming/merging details for FEM generation within a complete analysis deck.

Figure 11 and Figure 12 display a visualization of the MD-87 and Low Boom sketch files, respectively. By examining these figures, one can see color-coded 2D sketches for each component. Green lines represent RapidFEM SKIN3 cards while blue lines represent SKIN4 cards. Red lines indicate BEAM cards that are used, depending on the sketch, to represent ribs, spars, floors, or bulkheads.

Having a visualization capability has proven to be very useful for reducing both errors and debugging time involved in sketch file development. Although this is a time-intensive step, the goal is to perform this only once for each configuration. Afterward, any parametric changes to the original geometry will be automatically reflected within the sketch files.

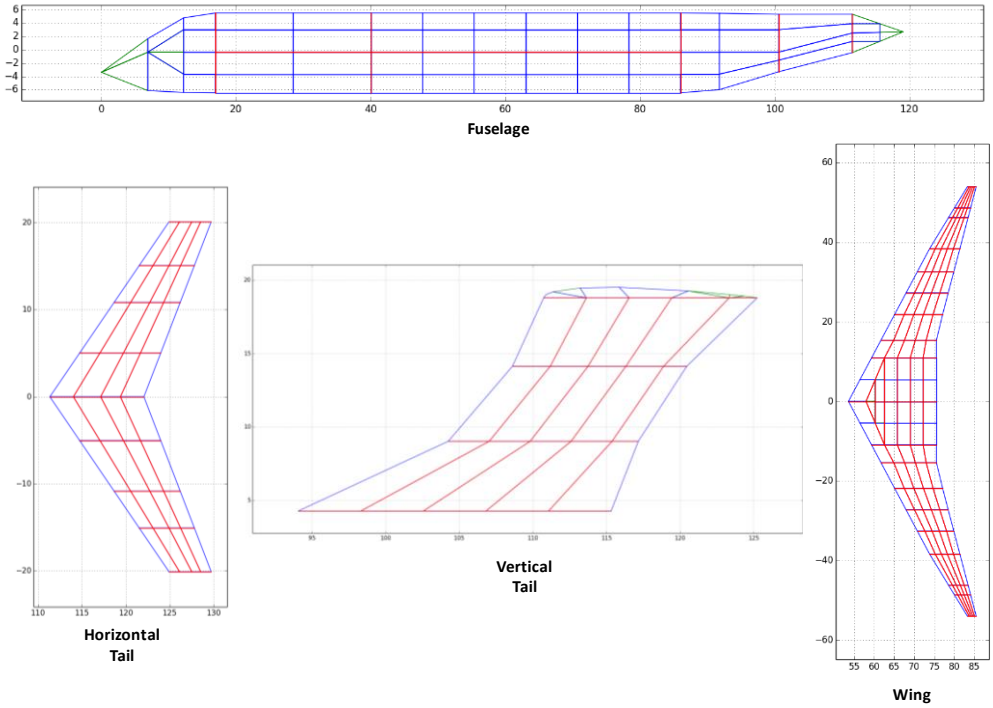

Figure 11: Visualization of MD-87 Component RapidFEM Sketch Files.

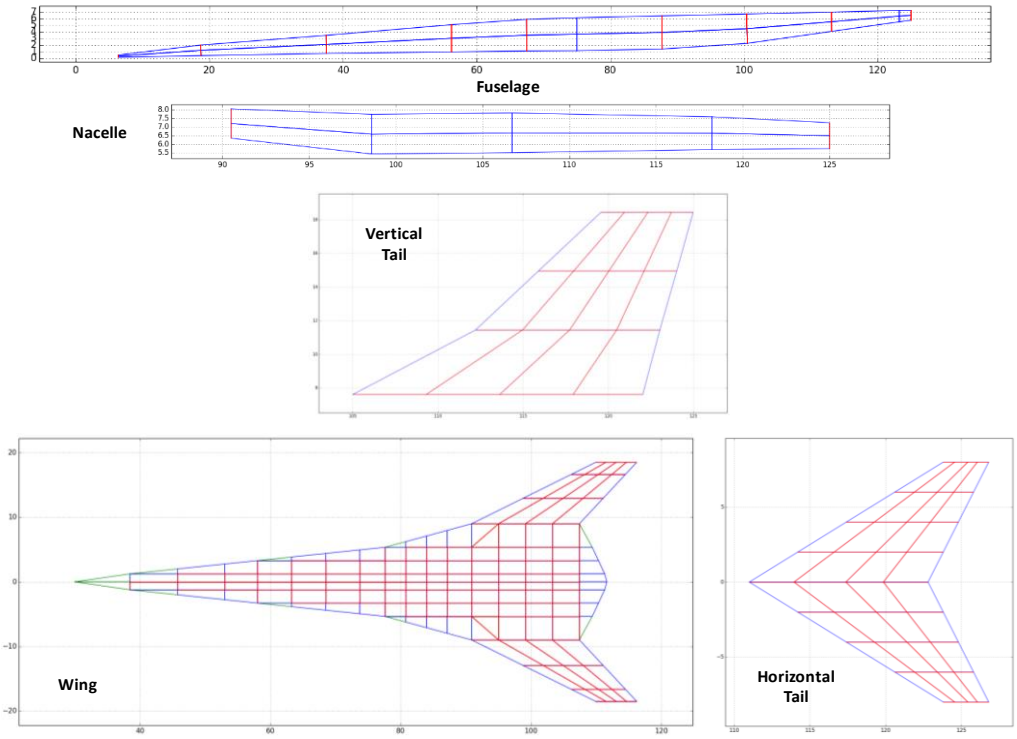

Figure 12: Visualization of Low Boom Component RapidFEM Sketch Files.

D. FEM Generation and Merging

The final step consists of executing RapidFEM to generate the component FEMs for each configuration and then merge them into a complete FEM. Figure 13 and Figure 14 show the MD-87 and Low Boom component FEMs along with the final merged FEM, respectively.

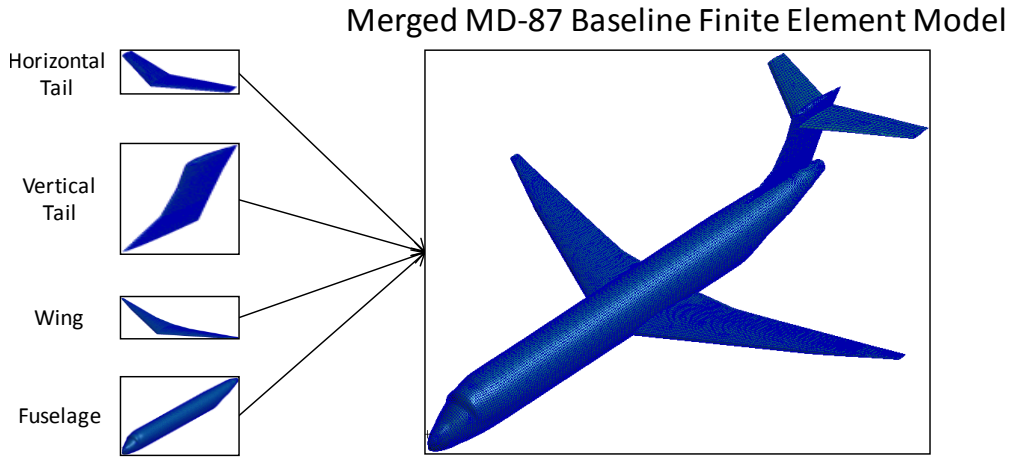

Figure 13: MD-87 Component FEMs and Merged FEM.

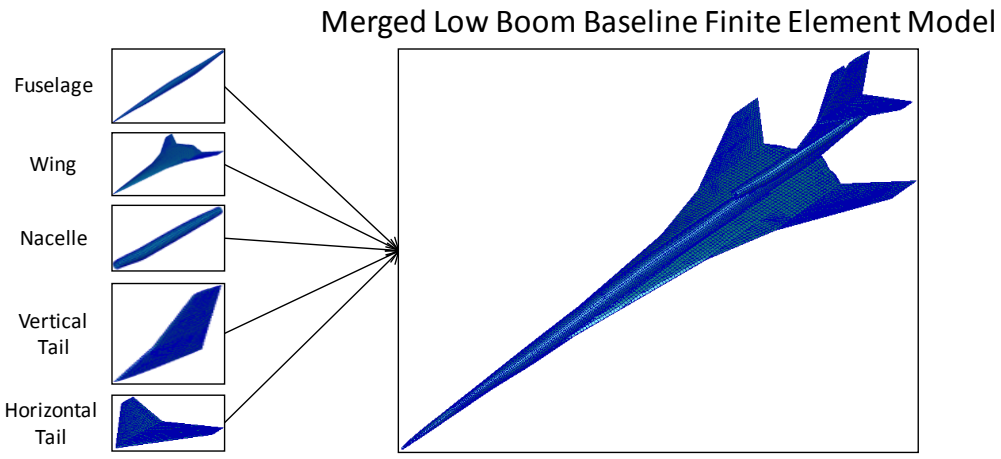

Figure 14: Low Boom Component FEMs and Merged FEM.

Figure 15 and Figure 16 show the details of the preliminary internal structural layout for the merged MD-87 and Low Boom FEMs, respectively. Bulkheads and floors can be observed in the fuselage, whereas ribs and spars can be observed in the wing, horizontal tail, and vertical tail.

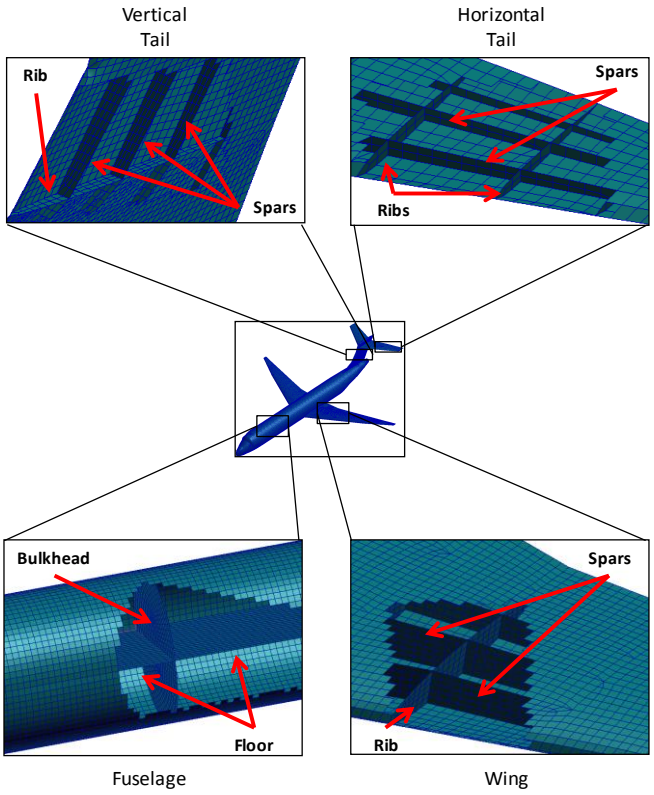

Figure 15: MD-87 Internal Structural Layout Details in Complete Merged FEM.

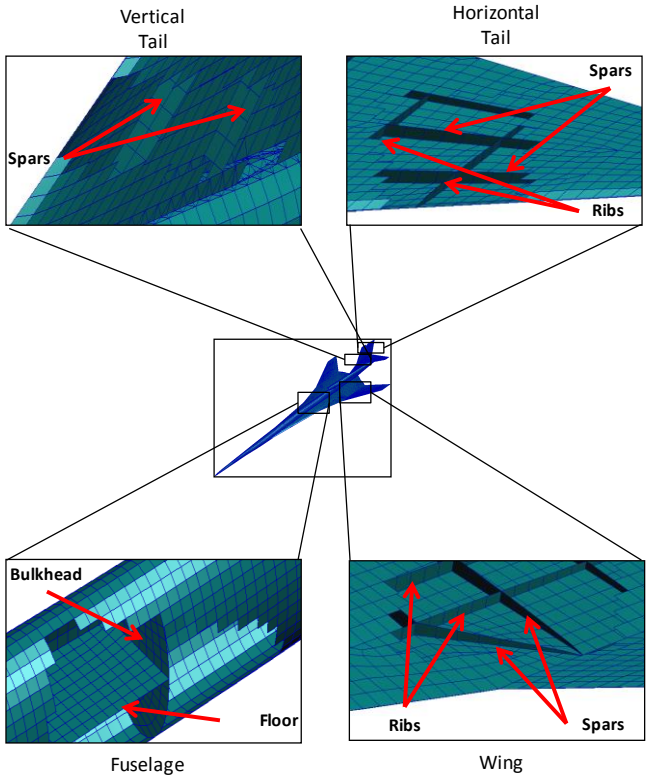

Figure 16: Low Boom Internal Structural Layout Details in Complete Merged FEM.

IV. Configuration Development

RapidFEM was used as the primary tool for developing the structural layout of the MD-87 and Low Boom configurations. The development process included property region layout and properly modeling the fixed mass contributions of each aircraft. By defining the property regions in each structural component, RapidFEM is able to search fewer elements and more easily trim special property regions after the merging process. Unique property regions are also necessary for specifying the NSM and thicknesses in each structure.

By leveraging RapidFEM's extended capabilities, the process is greatly expedited for generating parametric geometry and fixed mass representations, along with proper solution decks ready for analysis in Nastran. For further simplification, symmetric models for each configuration's components were used to expedite RapidFEM's parametric structural definition, merging, and trimming processes.

A. MD-87

After generating the basic FEMs for each of the components, their corresponding sketch files were then modified to define special property regions in order to expedite the merging and trimming process and to correctly spread the NSM across each structural component. RapidFEM also has built in cards to account for other fixed mass components such as engine attachments, landing gear attachments, and fuel tanks. Each of the cards was defined within the RapidFEM Sketch Files to generate a FEM with all the correct fixed masses.

RapidFEM's built in 'PROP' card allows for the components to be divided up into multiple property regions. For each of the components, the property identification number (RID) was chosen to satisfy both the NSM definition and merging and trimming process simplification. Figure 17 shows the property region layout for each of the components, with the colors representing various properties.

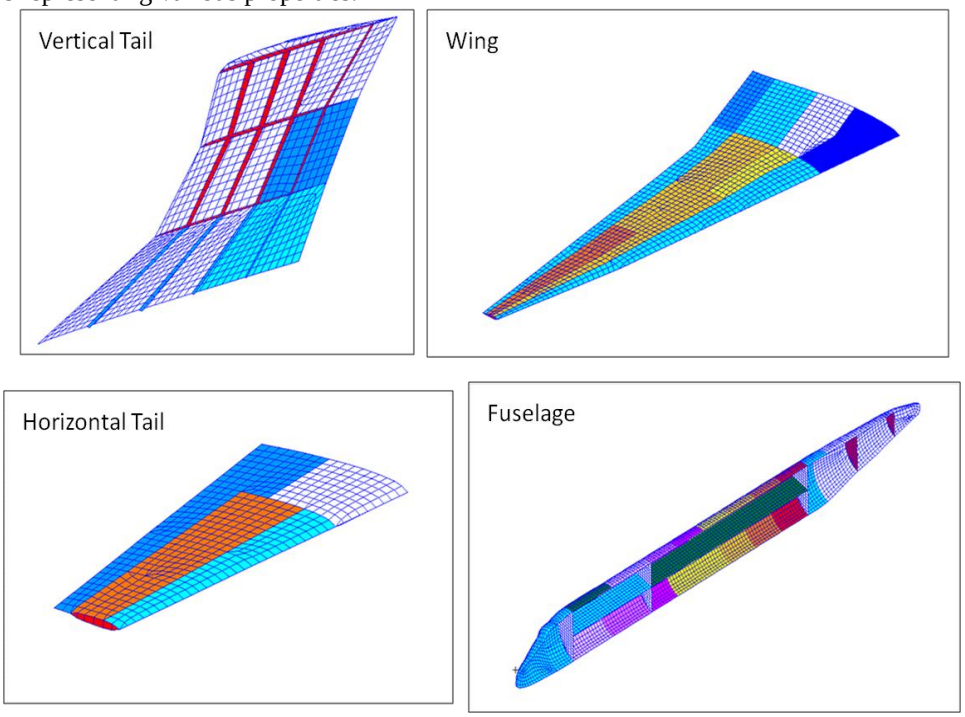

Figure 17: MD-87 Structural Component Property Region Layout.

In order to differentiate thicknesses between the beams and skins of the structure, unique RIDs were given to the spars/ribs of the wing and empennage as well as the bulkheads/floors of the fuselage. The fuselage properties were divided in a way to account for specific regions: the cockpit, top and bottom half of the cabin, and aft fuselage. The RIDs associated with skins making up the top and bottom half of the fuselage were further divided to allow Nastran's Solution 200 more freedom in sizing the fuselage structure. The wing was divided with properties making up the regions of the wing box, leading, and trailing edges. The horizontal tail properties were divided up in a similar manner as the wing, while the vertical tail properties were divided up to account for its merge with the fuselage and horizontal tail.

To accurately model the NSM distribution in each property region, the area of each property region must first be determined. The fixed mass in each property region is then divided by the area of each property region to give the NSM in pounds per square foot (psf). Table 1 provides a list of fixed mass contributions and corresponding weights and locations (Ref. 1). The 'Type' column shows a list of the corresponding RapidFEM cards used to model each of the fixed masses.

Table 1: MD-87 Fixed Mass Contributions to Fuselage and Wing (in Pounds).

Aircraft Component	MD-80	Type	Location
Nacelle	5340	ATTACHMENT	Fuselage
Nose gear	550	LDGR	Fuselage
Main gear	4790	LDGR	Wing
Engine	8820	ATTACHMENT	Fuselage
Nozzle system and $T_{reverser}$	1540	ATTACHMENT	Fuselage
Fuel system	640	NSM	Fuselage
Avionics and instruments	2130	NSM	Fuselage
Surface controls	2540	NSM	Wing/Emp
Hydraulic system	540	NSM	Fuse/Wing
Pneumatic system	1720	NSM	Fuse/Wing
Auxiliary power units (APU)	840	NSM	Fuselage
Oxygen system	220	NSM	Fuselage
Environmental control system (ECS)	1580	NSM	Fuselage
Anti-icing system	550	NSM	Wing
Furnishings	8450	NSM	Fuselage
Miscellaneous	3650	NSM	Fuselage
Fuel	14422	TANK	Wing
Payload	16103	NSM	Fuselage

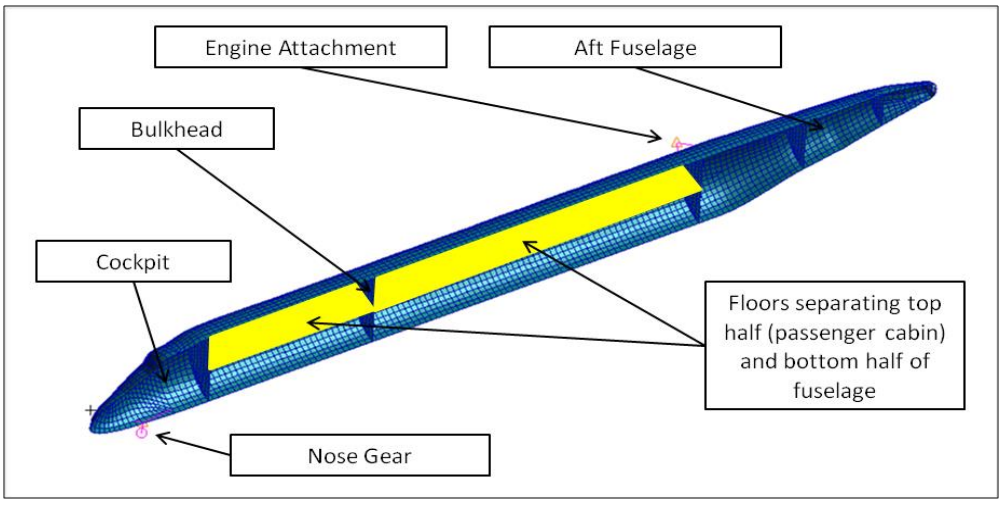

Figure 18: MD-87 Fuselage Layout.

The MD-87 fuselage is modeled with multiple bulkheads, which divide up the cockpit, cabin, and aft fuselage. Floors are also included in the passenger cabin, shown in yellow in Figure 18, and separate the top half of the fuselage from the bottom half. The engine, nozzle system, thrust reverser, and nacelle were all modeled using the RapidFEM 'ATTACHMENT' card, which attaches a point mass at the estimated Center of Gravity (CG) of the engine to the side of the aft fuselage. An approximate location of the engine's CG was determined by examining Figure 19 (Ref. 3). The nose gear of the fuselage was modeled in a similar manner using RapidFEM's 'LDGR' card, which creates a point

mass with a defined position along the x-axis and CG that simulates the landing gear of an aircraft. Figure 18 shows the fuselage FEM component with the respective engine and landing gear attachments. The remaining fixed mass in the fuselage was modeled as NSM using the 'PROP' card in RapidFEM.

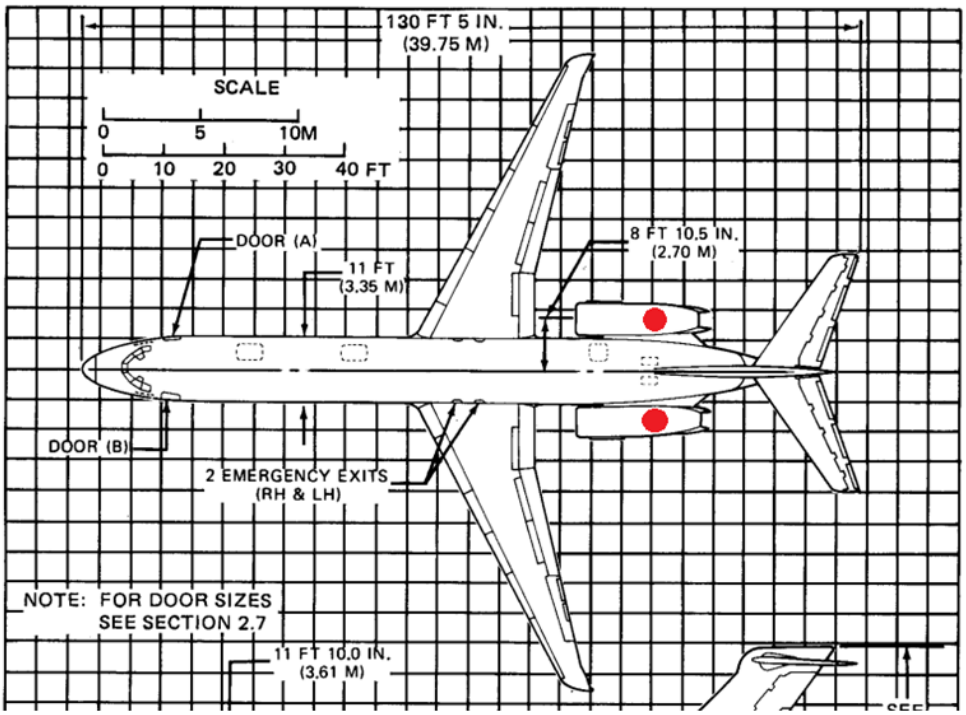

Figure 19: MD-87 Schematic Showing Approximated CG Position of Engine.

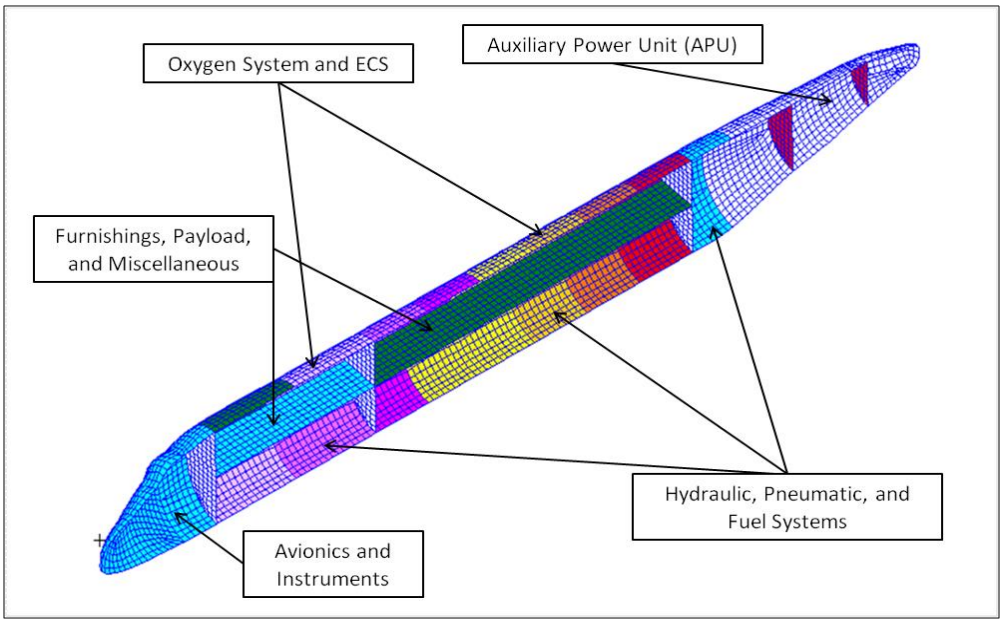

Figure 20: MD-87 Fuselage NSM Layout.

Figure 20 shows the NSM layout for the MD-87 fuselage. The hydraulic and pneumatic system masses were divided between the fuselage and wing, with most of the mass, along with the fuel system, contributing to the fuselage and spread across the bottom of the FEM, similar to the figures provided by the FAA and Aircraft Familiarization (Refs. 6 and 7). The Auxiliary Power Unit (APU) was spread across the aft fuselage, with the oxygen system and Environmental Control System (ECS) spread across the top half of the fuselage in the passenger cabin as referenced

in Refs. 7 and 8. The avionics and instruments were modeled as NSM in the cockpit of the fuselage, while the furnishings, payload, and the rest of the miscellaneous mass were spread across the floors in the passenger cabin.

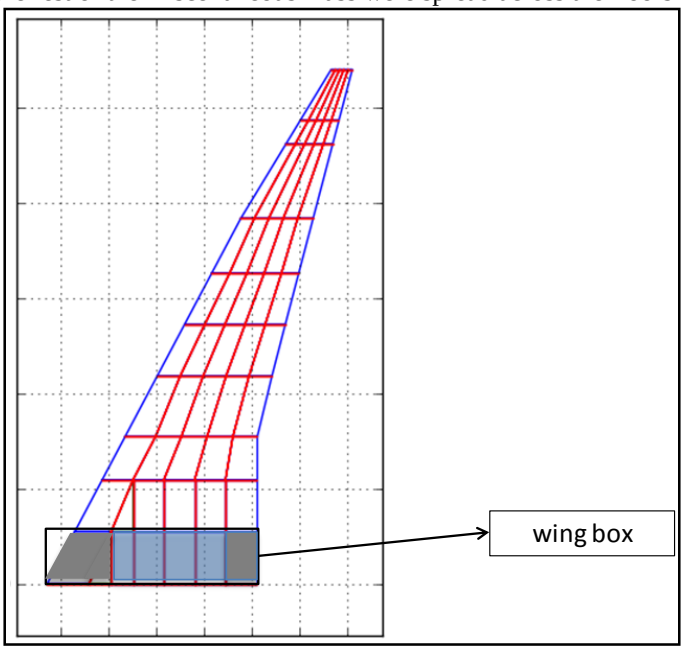

Figure 21: MD-87 Wing Layout.

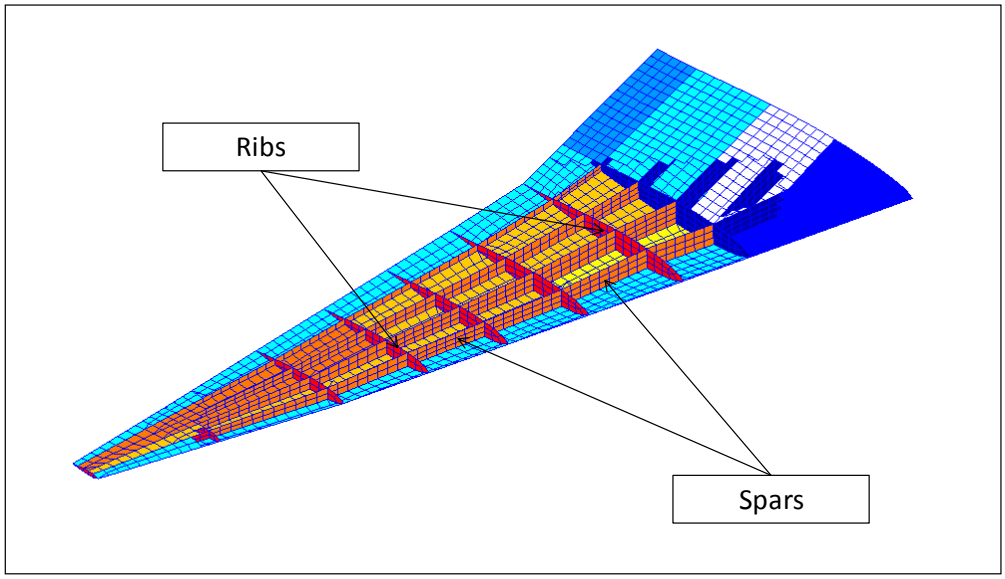

Figure 22: MD-87 Wing Internal Structure.

As seen in Figure 21, the MD-87 wing consists of spars (red vertical lines) and ribs (red horizontal lines) that run from the inboard to outboard part of the wing, along with a defined wing box. The corresponding FEM equivalent is seen in Figure 22. The MD-87 wing box in Figure 21 shows the carry-through structure in the blue shaded region and the trimmed structure denoted by the gray-shaded regions. To properly model the wing box in the fully merged MD-87 FEM, parts of the leading and trailing edge of the wing box were trimmed inside the fuselage, as shown in Figure 23. The trimming process was performed by defining a bounding box inside the fuselage and defining the RIDs of the wing to be trimmed inside that bounding box. Another trimming process was also performed in order to trim the portion of the fuselage that was merged inside the wing. Figure 24 shows the result of that trimming process. By properly defining the bounding box, RapidFEM is robust enough to determine the regions to trim by simply providing the associated RIDs.

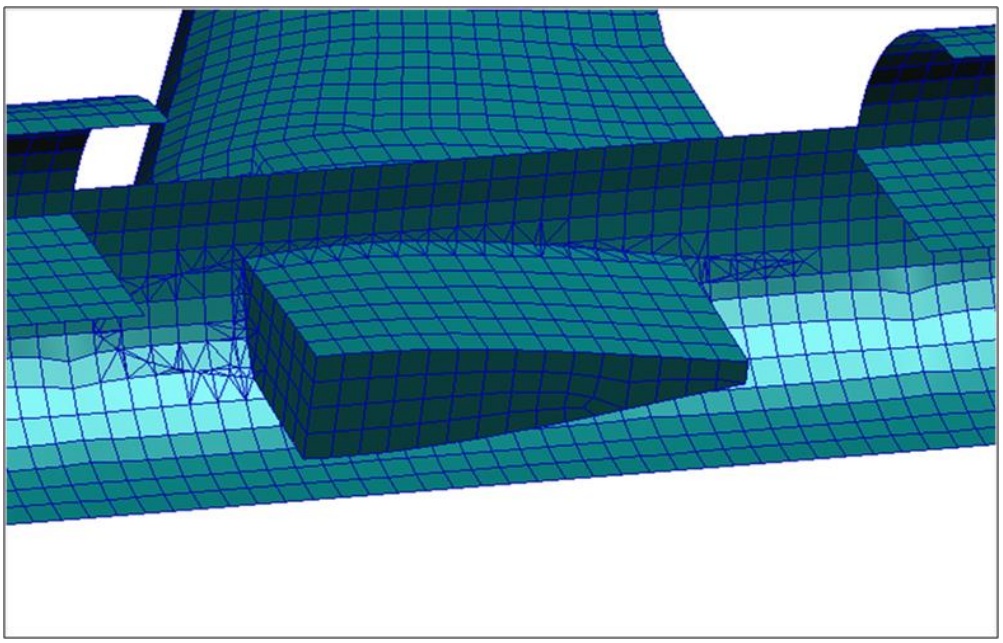

Figure 23: MD-87 Wing Box Trimmed Inside Fuselage.

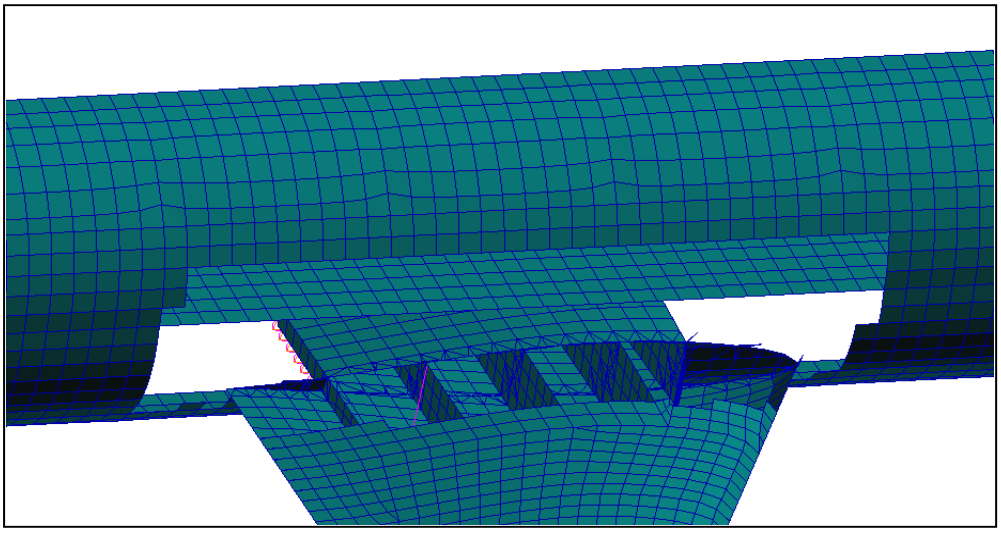

Figure 24: MD-87 Fuselage Trimmed Inside Wing.

The fuel was modeled in the wing using RapidFEM's 'TANK' card, which models the fuel as concentrated masses in a specified region. In RapidFEM, the fuel tank is defined by choosing the skins in the RapidFEM sketch file to make up the fuel tank and defining the weight of the fluid to be placed in the corresponding tank(s). RapidFEM is then able to generate a volume for the tank based on the chosen skins and fills the tank to the specified weight, assuming that the volume is sufficient enough to fit the weight of the fluid. The chosen fuel for this application was Jet A fuel, having a density of 50.194 pounds per cubic foot (lb/ft^3). The fuel distribution in the wing is shown in Figure 25.

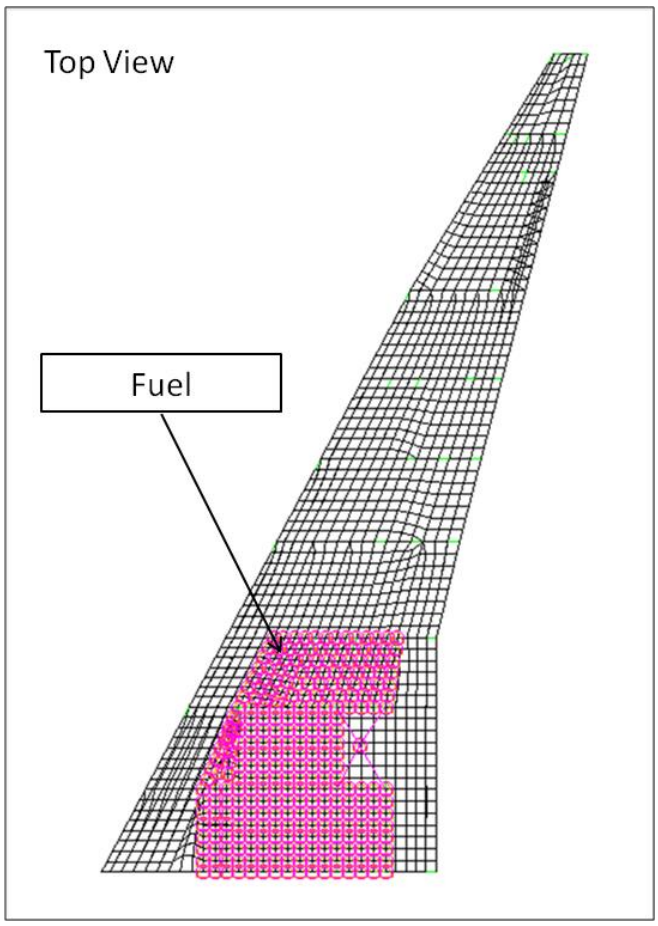

Figure 25: MD-87 Fuel Distribution in the Wing.

The main landing gear was modeled in a similar manner as the nose landing gear, using the built in 'LDGR' card in RapidFEM and is shown in Figure 26.

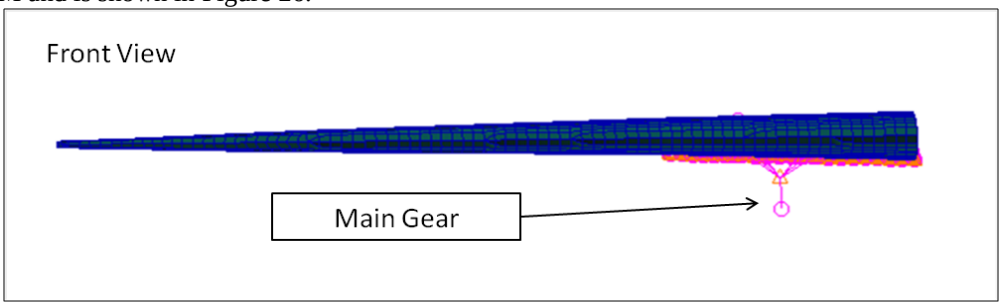

Figure 26: MD-87 Main Landing Gear on the Wing.

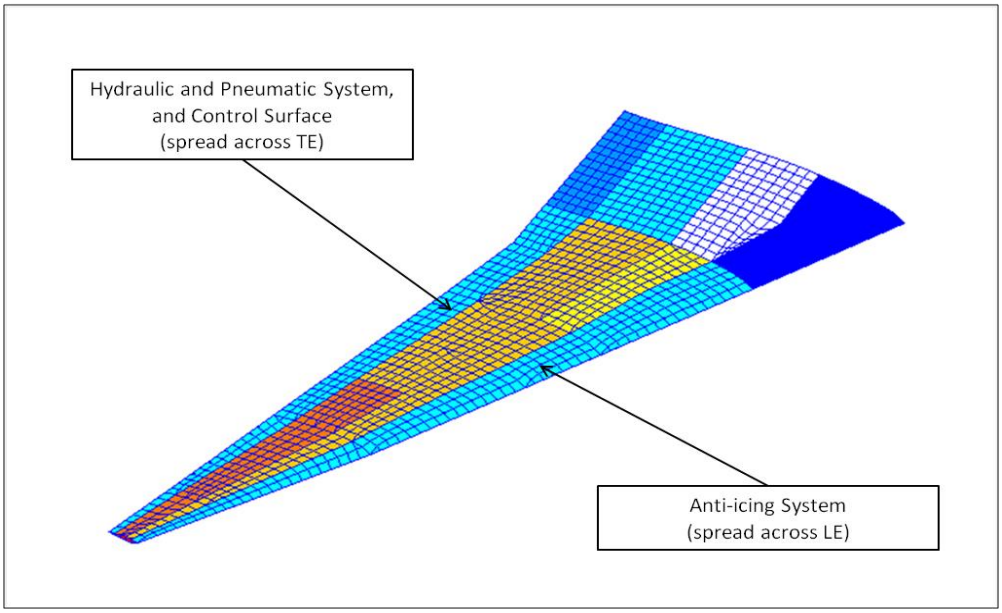

Figure 27: MD-87 Wing NSM Layout.

The total mass values for the fixed mass contributions to the wing are shown in Table 1. The total sum of the hydraulic and pneumatic systems masses was spread as NSM across the RIDs making up the trailing edge part of the wing, as shown in Figure 27 (Ref. 6). To account for the control surfaces, the mass was split between the wing, horizontal tail, and vertical tail. The portion of the control surface mass contributing to the wing was also spread across the trailing edge. The anti-icing system was spread across the leading edge of the wing (Ref. 9).

B. Low Boom Concept Demonstrator

At the highest level, the process for configuring the Low Boom was conducted in a similar manner as with the MD-87, by implementing the additional RapidFEM cards to account for NSM, attachments, and fuel. Due to limited data on the fixed mass contributions to the Low Boom, assumptions were made to determine the likely fixed mass components included in the Low Boom aircraft's total weight of 21,000 lb (Ref. 4). Table 2 provides a list of the assumed masses which were included and their corresponding mass values and locations, along with the RapidFEM cards used to model the mass components.

Table 2: Low Boom Fixed Mass Contributions in Fuselage and Wing (in Pounds).

Aircraft Component	Low Boom	Type	Location
Landing Gear, Nose and Main	1954.58	LDGR	Fuselage
Fuel System	111.61	NSM	Fuselage
Avionics and instruments	129.46	NSM	Fuselage
Surface Controls	339.82	NSM	Wing/Emp
Hydraulic system	152.22	NSM	Fuse/Wing
Pneumatic system	240.85	NSM	Fuse/Wing
Oxygen system	21.34	NSM	Fuselage
ECS	204.58	NSM	Fuselage
Anti-icing system	50.16	NSM	Wing/Emp
Fuel	7173.45	TANK	Fuse/Wing
Engine	2272	ATTACHMENT	Engine

To determine the values for each component, the average of six different aircraft's component weights relative to the TOGW were calculated in order to compute an estimate of the contribution of each fixed mass component to the Low Boom's total weight, as shown in Table 3. The six aircraft involved include the MD-87, DC-10-30, Boeing 737,

Boeing 727, Boeing 747, and Airbus A300. The main contributors to the mass of the Low Boom are the fuel and landing gear, which make up 34.16% and 9.31% of the total fixed mass, respectively.

Table 3: Low Boom Mass Contribution Approximation (LB column in Pounds).

Aircraft Component	MD-80	DC-10-30	737	727	747	A300	AVG	LB
Landing Gear, Nose and Main	0.0381	0.0852	0.1048	0.1105	0.1012	0.1186	9.31%	1954.58
Fuel System	0.0046	0.0078	0.0050	0.0071	0.0033	0.0042	0.53%	111.61
Avionics and Instruments	0.0152	0.0077	0.0054	0.0047	0.0027	0.0012	0.62%	129.46
Surface Controls	0.0181	0.0108	0.0203	0.0187	0.0098	0.0192	1.62%	339.82
Hydraulic System	0.0039	0.0047	0.0076	0.0089	0.0063	0.0123	0.72%	152.22
Pneumatic System	0.0123	0.0107					1.15%	240.85
Oxygen System	0.0016	0.0005					0.10%	21.34
ECS	0.0113	0.0049	0.0123	0.0124	0.0056	0.0121	0.97%	204.58
Anti-icing System	0.0039	0.0008					0.24%	50.16
Fuel	0.2812	0.4451	0.3006	0.3022	0.4671	0.2534	34.16%	7173.45

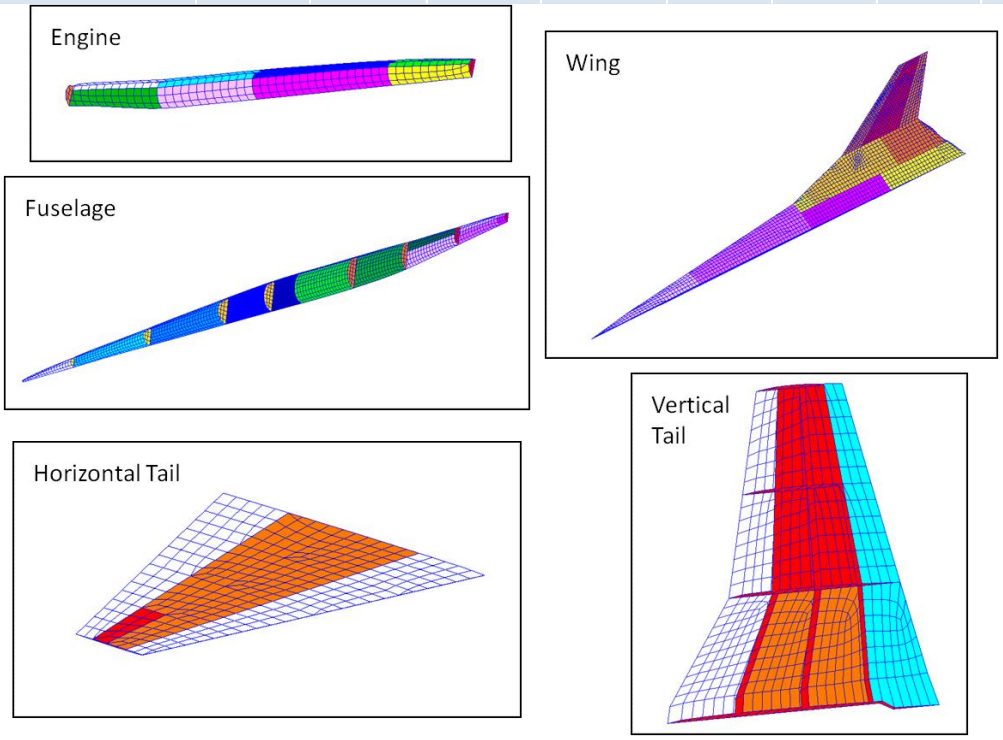

Figure 28: Low Boom Structure Component Property Region Layout.

Similar to the MD-87, the Low Boom properties were laid out to satisfy the merging, NSM, and initial thickness definition requirements. Figure 28 shows the property region layout for each of the Low Boom's structural components. The skins and beams are given unique RIDs to give the Nastran Solution 200 optimizer enough freedom to size the structural components. The wing RIDs are also divided up to distinguish between the leading and trailing edges as well as differentiate between the inboard and outboard ribs and spars. The same approach for defining the properties of the wing applies to the empennage as well. The properties for the engine nacelle were defined to satisfy the merging requirements with the fuselage and vertical tail.

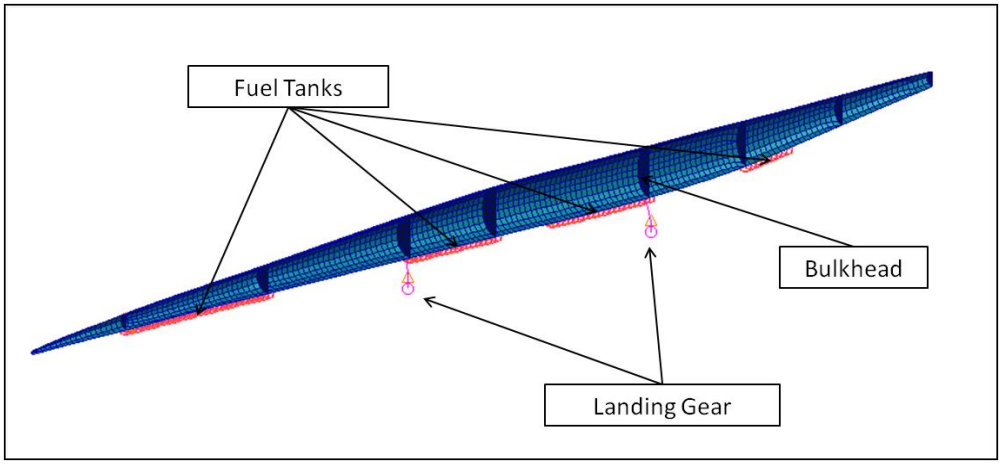

Figure 29: Low Boom Fuselage Layout.

The Low Boom fuselage layout contains bulkheads, fuel tanks, and landing gear, as shown in Figure 29. For simplicity, the mass of the pilot was modeled as NSM on a single property region of the wing, which is assumed to serve as the floor inside the fuselage after the merge process, as shown in Figure 30.

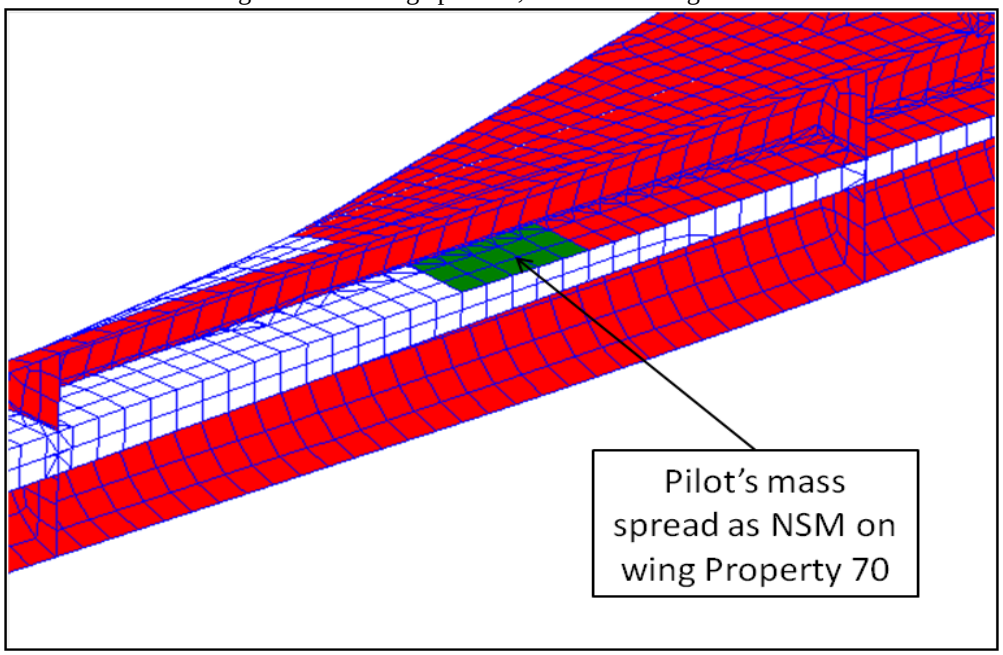

Figure 30: NSM Spread Over Wing to Simulate Pilot's Mass.

The total amount of fuel determined from Table 3 was split between the Low Boom fuselage and wing structures and modeled with the RapidFEM 'TANK' card, using Jet A fuel. To determine the fuel tank placement on the fuselage, a visual comparison was made to select the best possible skins to serve as the fuel tanks in reference to Ordaz et al. (Ref. 4). Figure 31 shows the comparison between the fuel tank configurations. The fuel tanks were chosen using pre-defined skins from the Low Boom wing RapidFEM sketch file. A direct comparison shows the part of the fuel in the fuselage placed too far forward. This is not a concern and is easily adjusted by configuring the skins to match the proposed fuel tanks.

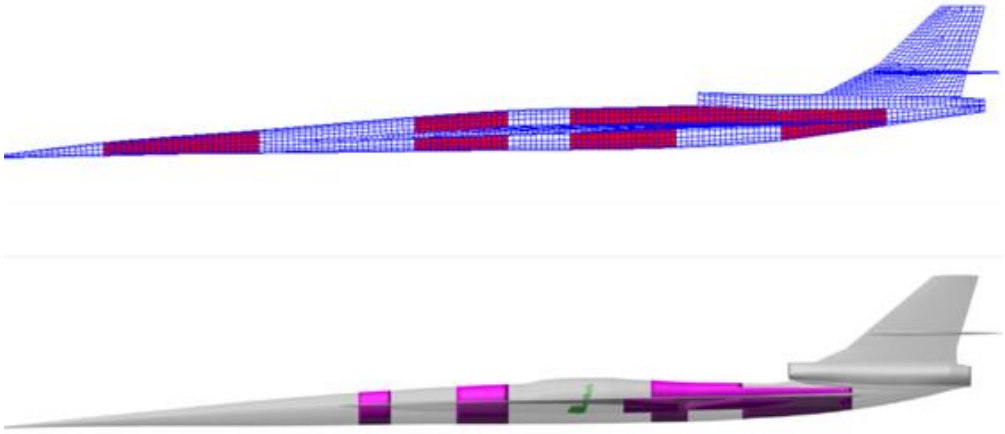

Figure 31: Low Boom Fuselage Fuel Tank Placement Comparison (Ref. 4).

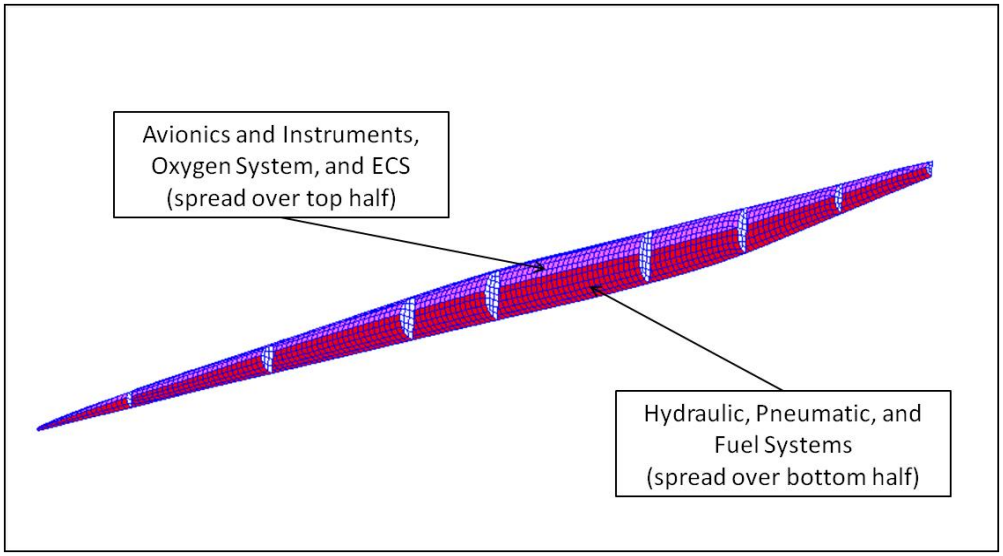

Figure 32: Low Boom Fuselage NSM Layout.

The NSM distribution in the fuselage was divided up and spread across two primary regions: the top and bottom half of the fuselage, as shown in Figure 32. The total sum of the avionics and instruments, oxygen system, and ECS were spread across the top half of the fuselage. The hydraulic and pneumatic systems were split between the fuselage and wing, with even mass contributions to both. Along with the fuel system, the hydraulic and pneumatic systems were spread across the properties making up the bottom half of the Low Boom fuselage.

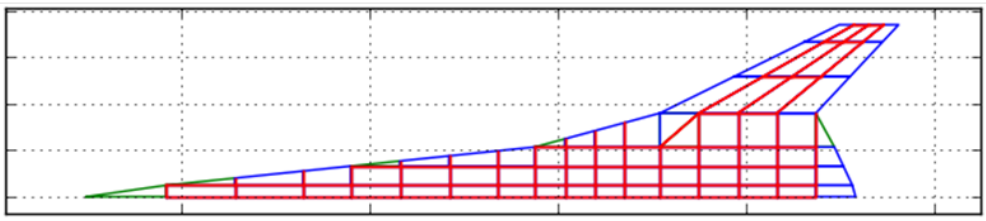

Figure 33: Low Boom Wing Layout.

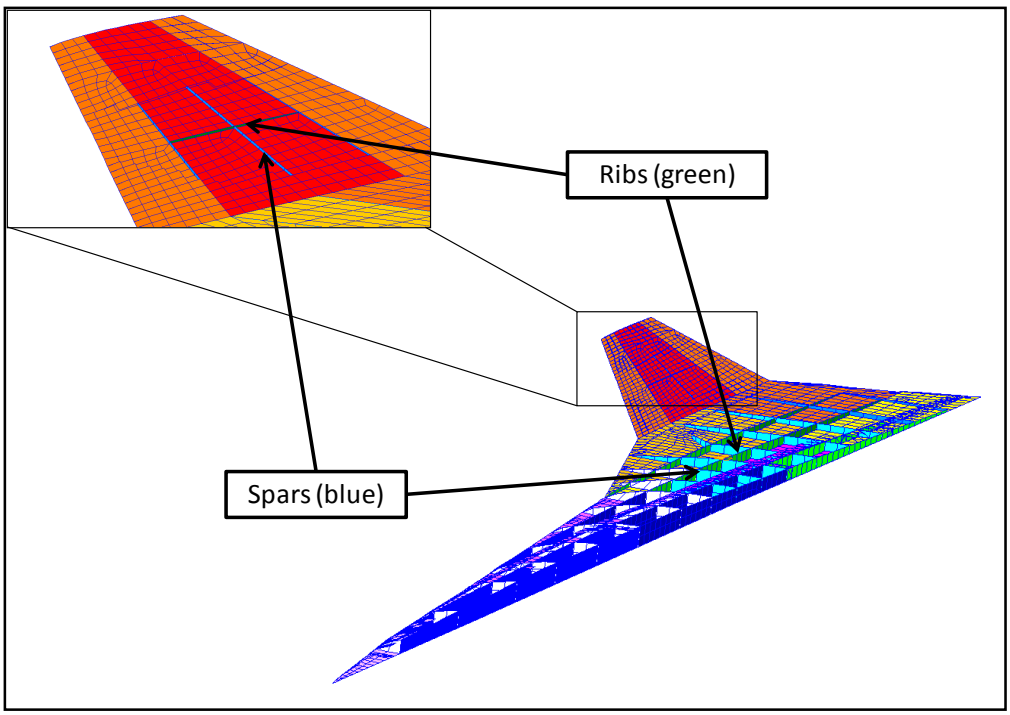

Figure 34: Low Boom Wing Internal Structure.

The unconventional design of the Low Boom wing features a variable sweep wing fitted with ribs (red horizontal lines) and spars (red vertical lines), shown in Figure 33. The corresponding FEM visualization is shown in Figure 34. There are two separate fuel tanks in the wing modeled through the 'TANK' card and are positioned with reference to Ordaz et al. (Ref. 4). Figure 35 shows the comparison of fuel tank placement in the wing.

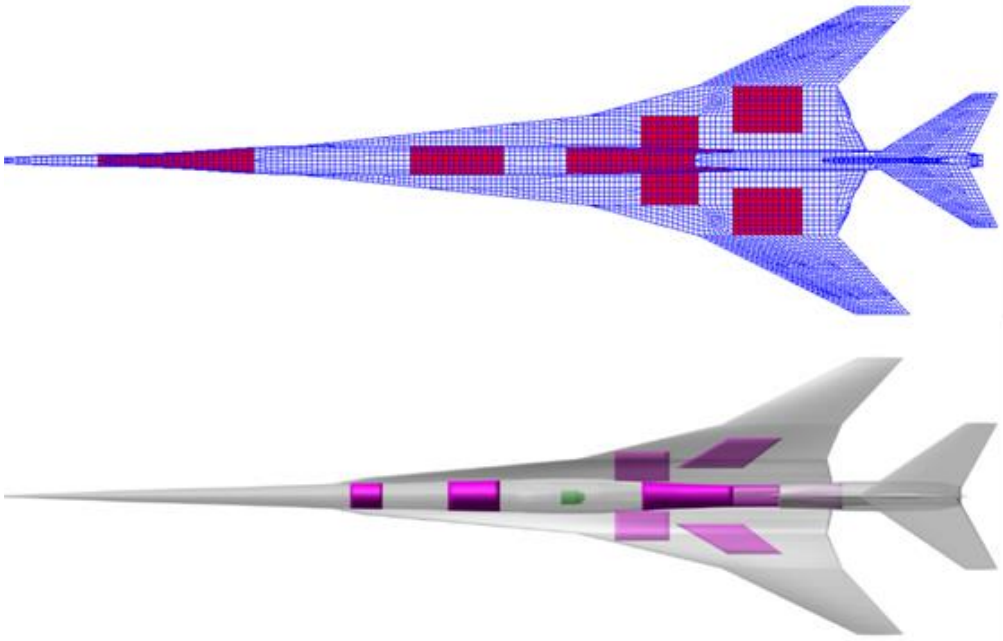

Figure 35: Low Boom Wing Fuel Tank Comparison.

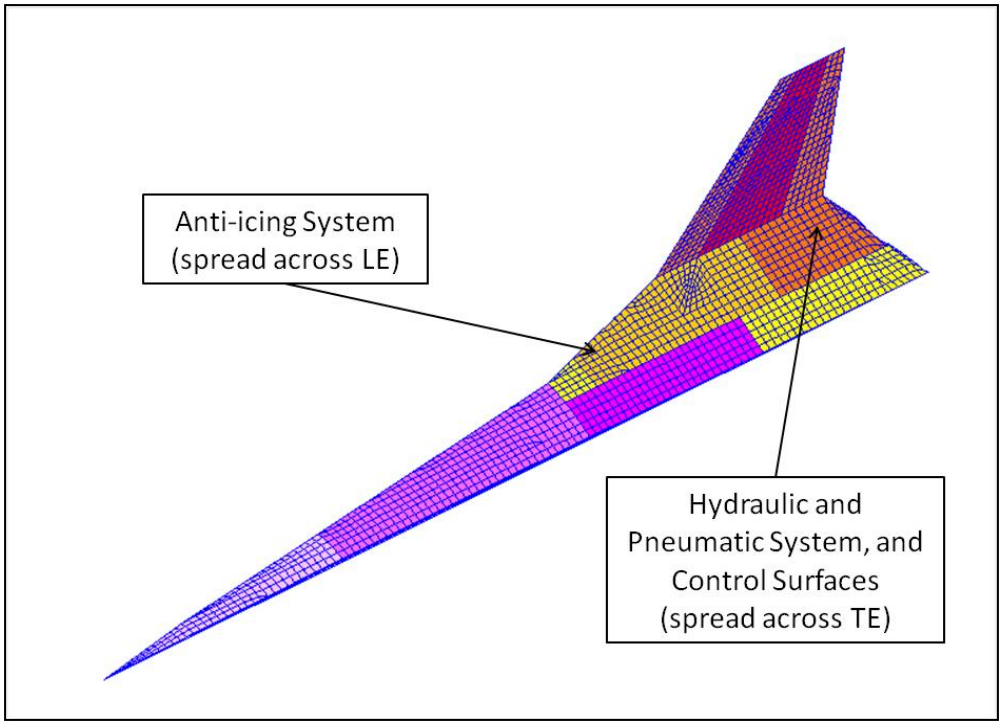

Figure 36: Low Boom Wing Layout.

A similar approach to NSM layout in the wing was applied for both the MD-87 and Low Boom. The NSM contribution in the wing was limited to the properties defining the leading and trailing edges, as shown in Figure 36. The anti-icing system was spread across the leading edge and the sum of the mass contributions from the hydraulic and pneumatic systems and the control surfaces were spread throughout the wing trailing edge.

V. Example Applications

A. MD-87: Example Problem Description

The goal for the analysis effort was to arrive at a substantial estimate for the MD-87 structural weight, primarily for the fuselage and wing structural components. The problem statement for the analysis included assuming a uniform metallic structure (aluminium), fixed non-structural mass, two separate load cases as specified in FAA Regulations (FAR) Part 25, and defined stress constraints or allowable stresses. The material used for the MD-87 structure was aluminium alloy 7068, with an allowable tensile stress (F_{tu}) around 100 kilo-pounds per square inch (ksi) (Ref. 10). Two load cases were considered to size the fuselage and wing structural components, as defined by FAR Part 25 (Ref. 11). These load cases included the 2.5g pull-up maneuver and the abrupt pitch maneuver. Table 4 provides the flight conditions for each of the two load cases performed in Nastran for the MD-87. The flight conditions include high subsonic speed coupled with high dynamic pressure. In the analysis. the fuselage was sized by the fatigue allowable of 21 ksi. The assumed life was equal to 50000 cycles, scatter factor of five and a K_T equal to three. The wing was sized by one-third of the F_{tu} of aluminium alloy 7068, which is approximately 34.3 ksi. It is important to note that the effects of turbulent gust loads, fuselage stiffeners, rings, frames, and flutter constraints were implicitly considered within the allowables.

Table 4: MD-87 Flight Conditions for the Load Cases.

Load Case	Mach Number	Altitude (ft)
2.5g Pull-Up	0.84	Sea Level
Abrupt Pitch	0.84	Sea Level

The MD-87 baseline configuration was optimized using Nastran's Solution 200 optimizer. Static aeroelastic analysis (Nastran Solution 144) was performed in conjunction with the optimization for each of the load cases. The design variables consisted of the property region thickness over the entire FEM model, with the initial thicknesses

defined in the RapidFEM 'PROP' cards. The thicknesses were constrained by a minimum gage of 0.1 inches, while the stresses were constrained by the allowables mentioned above.

B. MD-87: Baseline Optimization Results

The MD-87 baseline optimization result for the wing Von Mises stress can be seen in Figure 37. The results confirm that the wing is indeed sized by the allowable of 34.3 ksi, as a result of the 2.5g pull-up maneuver. Figure 37 shows the red hotspots, as pointed to by the arrows, at the specified allowable, which sizes up the thicknesses of the wing in the corresponding sections. As a result of the 2.5g pull-up maneuver, the wing tends to deflect upwards, with a max deformation of 3.19 feet at the wing tip, as shown in Figure 38.

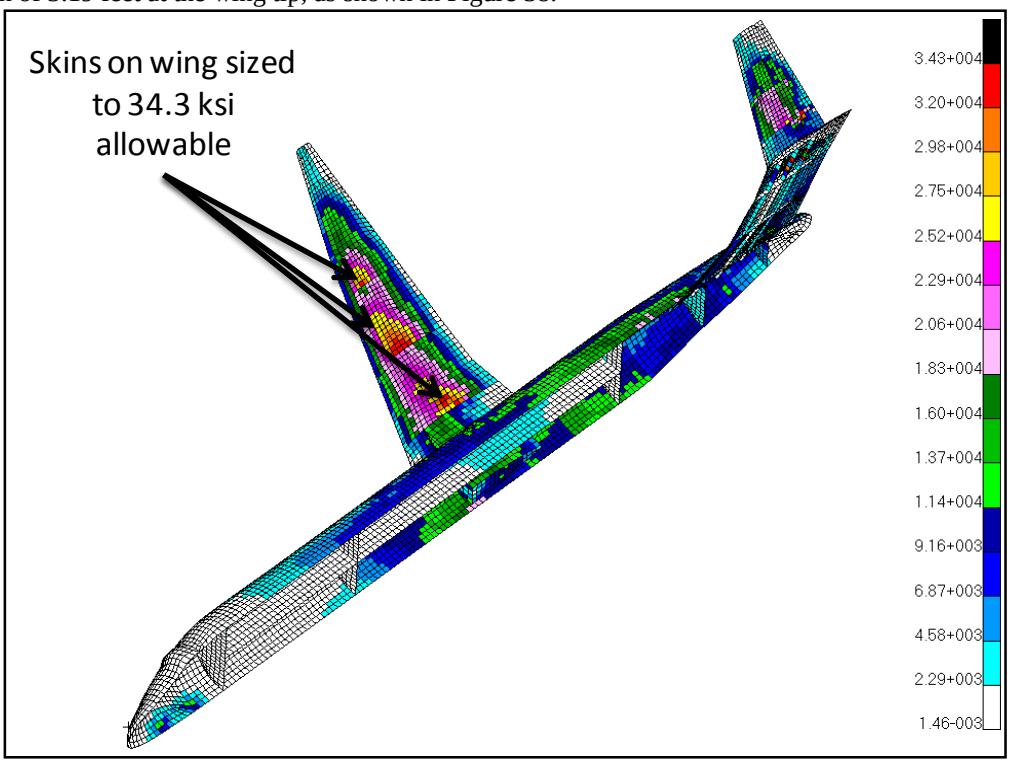

Figure 37: MD-87 Baseline Optimization Wing Stress (Von Mises) Distribution.

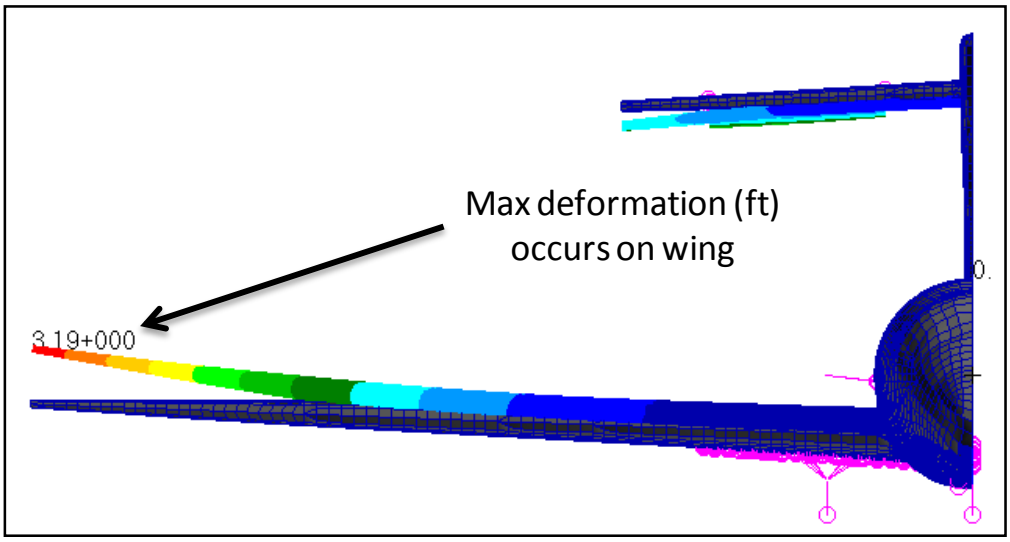

Figure 38: MD-87 Baseline Optimization Wing Maximum Deformation.

The results show the fuselage being sized by the allowable of 21 ksi, as a result of the abrupt pitch maneuver. Figure 39 shows the regions of the fuselage where the maximum stresses occur, denoted by the red hot spots as pointed to by the arrows. Due to the abrupt pitch, the fuselage stress is a maximum around the bottom half of the fuselage. Figure 39 also shows the deformation, at a scale factor of twenty, with the nose of the fuselage drooping, and the aft fuselage and empennage deflecting downwards due to the load applied on the empennage in accordance with the elevator deflection.

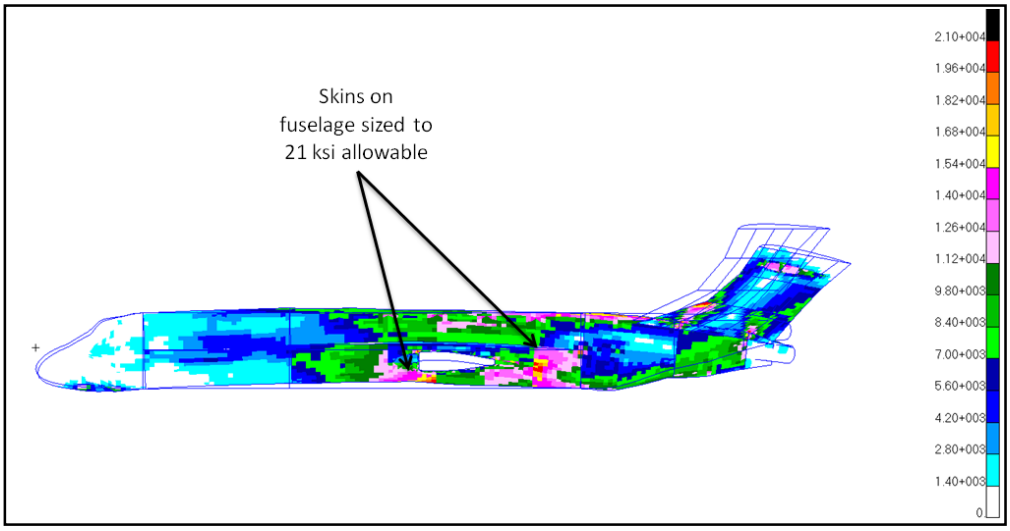

Figure 39: MD-87 Baseline Optimization Fuselage Stress (Von Mises) and Deformation.

The summarized result for the MD-87 weight statement is provided in Table 5. The data in Table 5 shows the published data for each of the structural components as well as the total mass for each structural component's NSM, including engine attachments, landing gear, and fuel tanks. Table 5 also includes the results from the PBWeight analysis along with the corresponding percent errors between the published values and those of PBWeight.

Table 5: MD-87 Baseline Optimization Weight Statement.

	Published Data (Ref. 2)	PBWEIGHT	% Error
Fuselage Structure (lb)	16150	15001	7.1%
Fuselage NSM (lb)	67548	67548	0.0%
Wing Structure (lb)	15560	15698	0.9%
Wing NSM (lb)	36979	36979	0.0%
Tail Structure (lb)	3320	5543	67.0%
Tail NSM (lb)	443	443	0.0%
Total Structure (lb)	35030	36242	3.5%
Total Takeoff Gross Weight (lb)	140000	141212	0.9%

PBWeight predicted a fuselage structural weight roughly a thousand pounds shy of the published value, while the predicted weight for the wing was just slightly over-predicted, with less than one percent error. However, the tail structure weight was well over-predicted, with the large error due to a bad element driving the optimizer to size the whole property region in a portion of the horizontal tail to a large thickness. Although the tail error was significantly large, the overall error in the total TOGW was less than one percent, as shown in Table 5.

C. MD-87: Single Parameter Optimization Results

Figure 40 presents the results for the MD-87 fuselage length variation study. The fuselage length was varied between 100 to 150 feet, while the fuselage height was kept fixed at 11.95 feet. Overall, PBWeight predictions for fuselage structural weight show good agreement with the results tabulated from Nicolai's empirical equations. As the length of the fuselage increases, the weight increases as well. It is important to note that Nicolai's values were computed using the TOGW computed by PBWeight, hence the non-smooth trend seen in Figure 40.

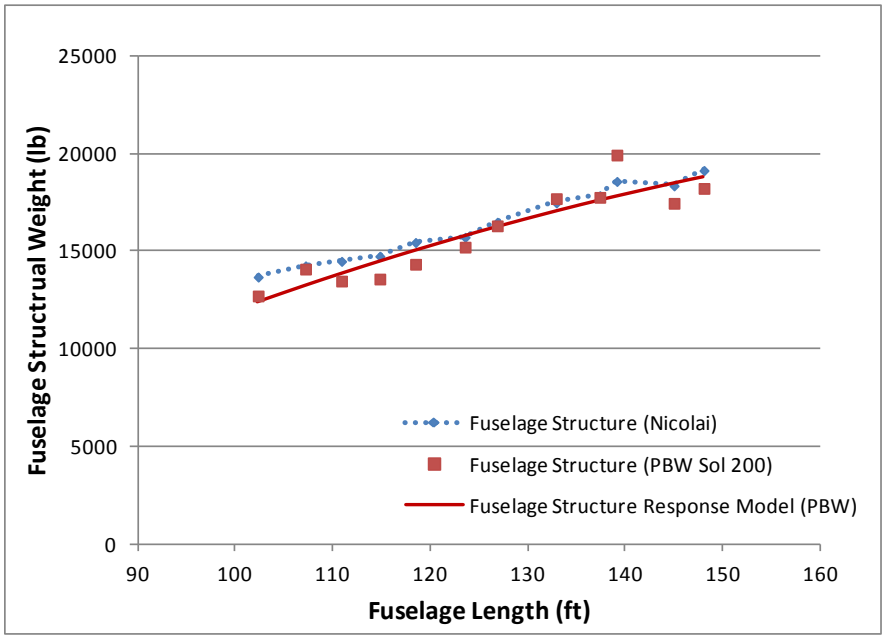

Figure 40: MD-87 Fuselage Length Variation Study.

A fuselage height variation study was also conducted for the MD-87. The fuselage height was varied between 5 to 15 feet, while the fuselage length was fixed at 119.08 feet. Unlike the fuselage length variation study, Figure 41 shows a noticeable disparity in the trend between PBWeight's predicted weight and Nicolai's empirical equations.

Nicolai's empirically-based equation for fuselage weight shows a large increase in structural weight as the fuselage height is decreased due to the $(L/H)^{0.71}$ term in his equation, shown below. PBWeight's trend also shows an increase in structural weight as fuselage height is decreased, but the increase is minimal since a large portion of the fuselage skin is at the minimum gage of 0.1 inches. The interesting takeaway from Figure 41 is the noticeable difference in fuselage structural weight with heights that appear to be outside the normal height distribution of conventional transport aircraft, which are contained within Nicolai's empirical database. However, PBWeight does show good agreement with Nicolai near the baseline height of the MD-87, which is approximately 12 feet.

Equation 1: Nicolai Empirical Fuselage Weight Equation

$$W_{fuselage\ -comm} = 10.43 * K_{INL}^{1.42} (q * 10^{-2})^{0.283} (W_{TO} * 10^{-3})^{0.95} (L/H)^{0.71}$$

Overall, the fuselage length variation study showed good agreement between PBWeight and Nicolai's empirical equations, particularly because the lengths chosen were well within the length requirements of conventional transports. On the other hand, the fuselage height variation study showed that the results between PBWeight and Nicolai tend to diverge when the heights differ from that of conventional transports, but converge at fuselage heights

modeled within the conventional transport database.

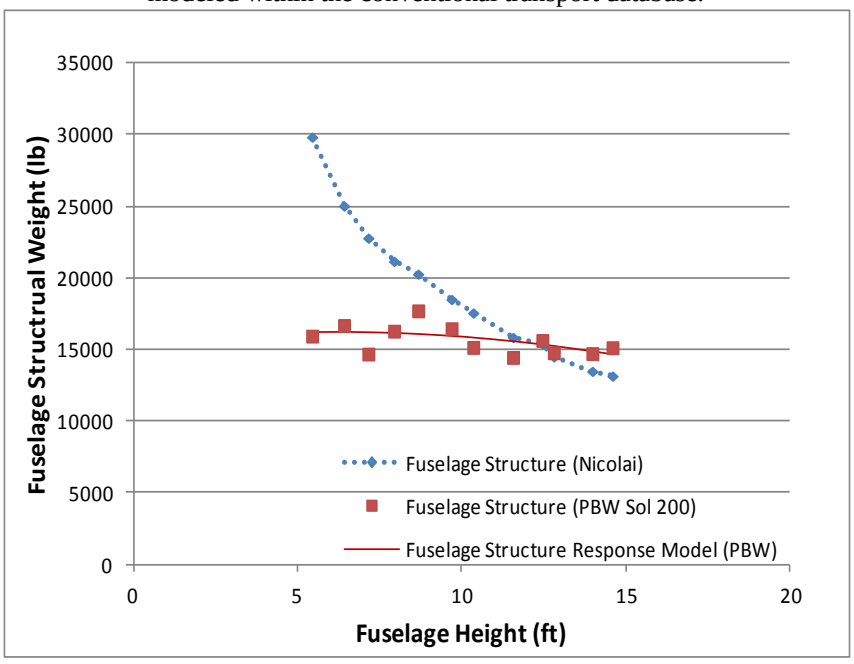

Figure 41: MD-87 Fuselage Height Variation Study.

D. Low Boom Concept Demonstrator: Example Problem Description

The Low Boom problem statement is similarly defined to the MD-87's problem statement, with the only major difference being the flight conditions between the two. The Low Boom was modeled with a uniform aluminum structure, aluminum alloy 7068, with fixed NSM, as determined in Table 3. The static aeroelastic analysis included the 2.5g pull-up maneuver as well as the abrupt pitch maneuver with the flight conditions provided in Table 6. The Low Boom flight conditions simulated cruise flight at high altitude and supersonic speed, and were directly referenced from Ordaz et al. (Ref. 4). The allowables for sizing the Low Boom fuselage and wing were 21 ksi and 34.3 ksi, respectively. The effects of turbulent gust loads, fuselage stiffeners, rings, frames, and flutter constraints were all considered implicitly within the allowables.

Table 6: Low Boom Flight Conditions for the Load Cases.

Load Case	Mach Number	Altitude (ft)
2.5g Pull-Up	1.6	50000
Abrupt Pitch	1.6	50000

E. Low Boom Concept Demonstrator: Baseline Optimization Results

The Low Boom baseline optimization results for the wing Von Mises stress is shown in Figure 42. Due to the 2.5g pull-up maneuver, the Low Boom wing is sized by the 34.3 ksi allowable. Like the MD-87, the maximum allowable stress sizes the skins of the wing structure accordingly in the various sections defined from the inboard section of the wing to the outboard. Due to the slenderness of the Low Boom wing, the max deformation occurs at the wing tip with a magnitude of around seven feet, as shown in Figure 43.

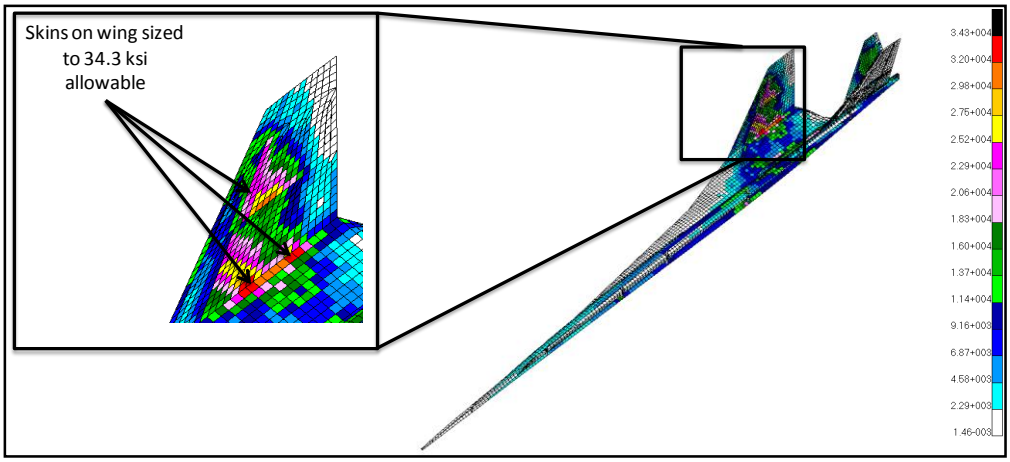

Figure 42: Low Boom Baseline Optimization Wing Stress (Von Mises) Distribution.

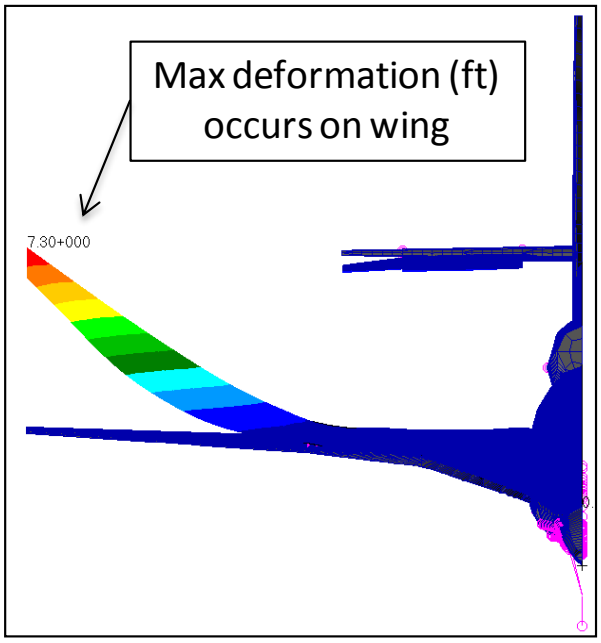

Figure 43: Low Boom Baseline Optimization Wing Maximum Deformation.

The Low Boom baseline optimization results for the fuselage Von Mises stress is shown in Figure 44. The fuselage is sized according to the 21 ksi allowable at the locations corresponding to the landing gear and engine attachments, as denoted by the arrows. The abrupt pitch maneuver causes the Low Boom fuselage nose to droop while the aft fuselage and empennage structure deflect downwards due to the applied loads and elevator deflection, similar to the deformation seen in the MD-87 results.

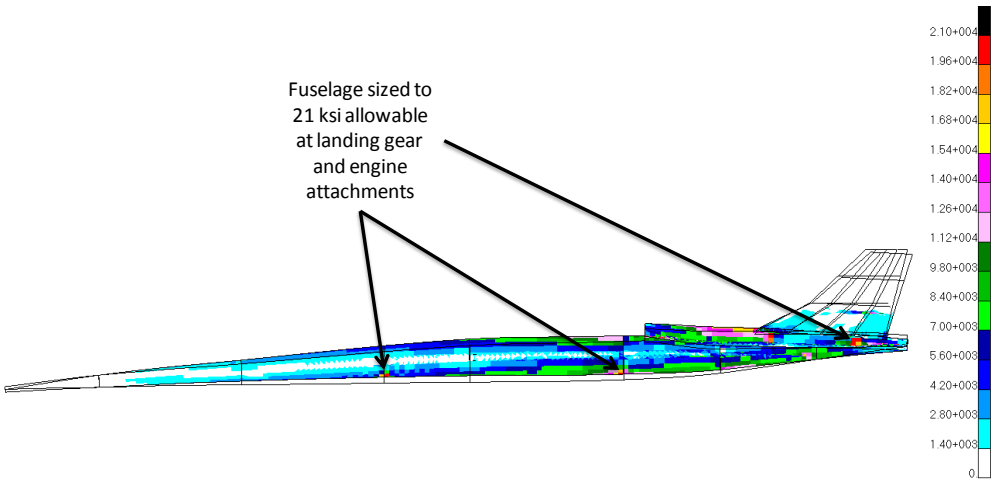

Figure 44: Low Boom Baseline Optimization Fuselage Stress (Von Mises) and Deformation.

Table 7 provides the summarized result for the Low Boom weight statement. The only published data provided for the Low Boom was the weight of the engine and the TOGW, as referenced in Ordaz et al. (Ref. 4). The PBWeight column provides the data for the NSM, as determined in Table 3, and the structural component weights determined from the Nastran Solution 200 optimizer. PBWeight predicts the total structure weight to be just less than 9000 pounds with the TOGW just 2.2% shy of the published weight value. Overall, the PBWeight results show promise in being able to predict the weight of an unconventional structure, such as the Low Boom Demonstrator Concept.

Table 7: Low Boom Baseline Optimization Weight Statement.

	Published Data (Ref. 3)	PBWEIGHT	% Error
Fuselage Structure (lb)	-	1805	-
Fuselage NSM (lb)	-	7400	-
Wing Structure (lb)	-	5164	-
Wing NSM (lb)	-	2752	-
Tail Structure (lb)	-	1038	-
Tail NSM (lb)	-	227	-
Engine Structure (lb)	-	804	-
Engine NSM (lb)	2272	2272	0.0%
Total Structure (lb)	-	8811	-
Total Takeoff Gross Weight (lb)	21000	21462	2.2%

F. Low Boom Concept Demonstrator: Single Parameter Optimization Results

A fuselage length variation study was conducted to compare the results of Nicolai's weight values to PBWeight results for an unconventional fuselage structure of varying lengths and fixed height. The results, shown in Figure 45, show a similar trend of increasing weight associated with increasing fuselage length, however the values for Nicolai are about twice the values determined by the PBWeight analysis. This is due to the fuselage height being fixed at 5.02 feet, which is outside the normal height distributions of conventional transports, and thus is not properly captured within Nicolai's empirical database. Unless the fuselage height is within the height limits of a conventional transport, the weight values between Nicolai and PBWeight will not converge to each other.

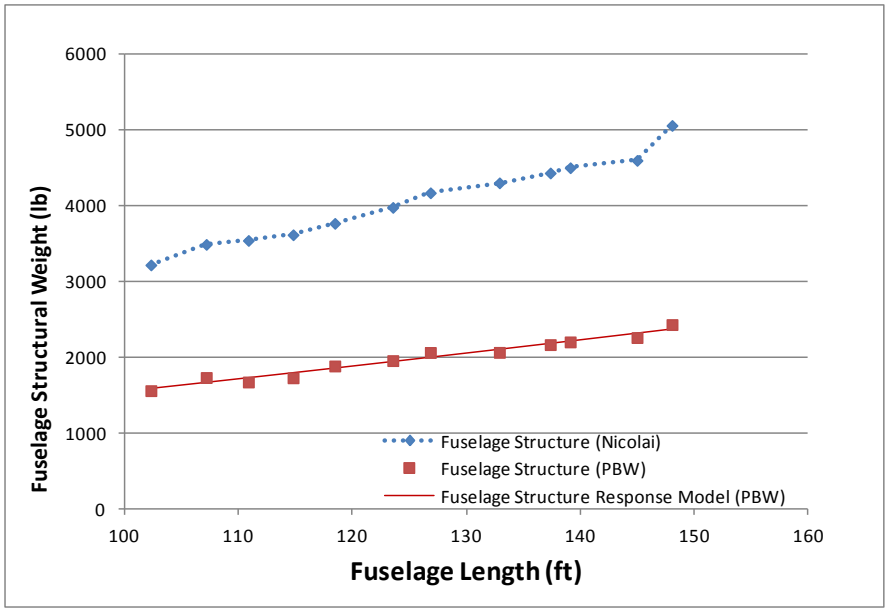

Figure 45: Low Boom Fuselage Length Variation Study.

A fuselage height variation study was also conducted with a fixed length of 125 feet. The results are presented in Figure 46, which shows different trends between Nicolai's empirical equation and PBWeight. Nicolai's results for the height variation study follow the trend dictated by the exponential factor in Equation 1. Interestingly, PBWeight shows an increasing trend for the weight as the fuselage height increases. The heights in the variation study lie outside Nicolai's empirical database for conventional transports, however, Figure 46 shows that as the heights approach the typical conventional transport height, the two curves seem to converge toward an agreeing weight.

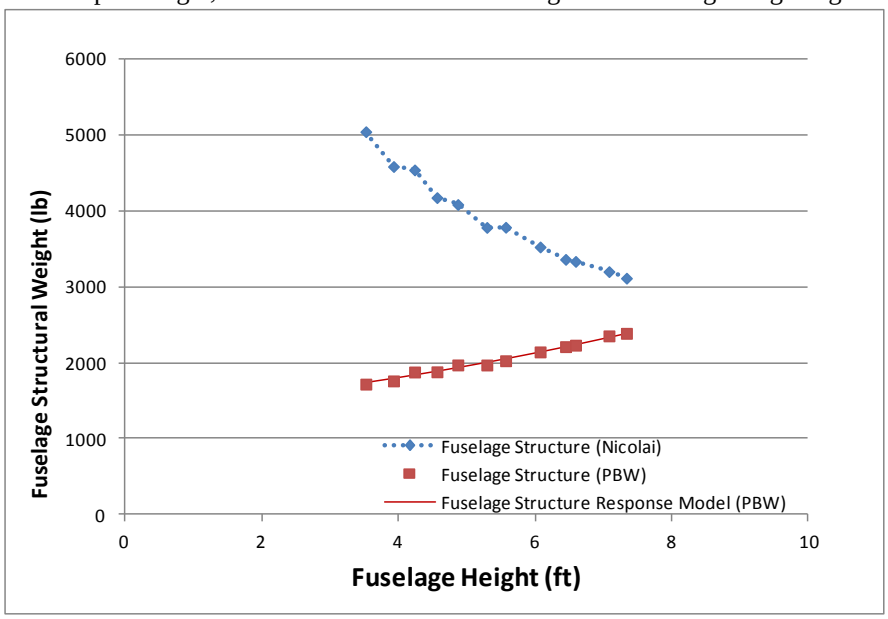

Figure 46: Low Boom Fuselage Height Variation Study.

Overall, the results for both variation studies of the unconventional Low Boom vehicle show interesting disparities between Nicolai's empirical equations and PBWeight. Although the trends were similar in the fuselage length variation study, Nicolai's equations consistently predicted larger weight values than PBWeight. The height variation study showed two very different trends, with PBWeight showing increasing weight as the fuselage height was increased, while Nicolai's equation followed the exponential trend. It appears the Low Boom fuselage structure captures a design that is not representative of the majority of aircraft within the empirical database of conventional

transports. One major difference is the overall shape of the Low Boom fuselage, which does not resemble the typical cylindrical shaped fuselages seen in most conventional transports. The design of the Low Boom fuselage is more consistent with a conical shape. Overall, the results show that the physics-based approach to estimating weight tends to agree with empirically-based equations when parameters fall within the values existing in the historical database, but diverge when considering parameters outside the historical database.

F. Multi-Parameter Optimization

Currently, PBWeight is also capable of performing simultaneous parametric variation studies. It is able to automatically generate animations of the stress results as well as weight statements throughout the design space, promoting a visual understanding of the parametric variation results. The current multi-parameter variation capabilities will be further extended to include integration with the OpenVSP parametric geometry software. By integrating multi-parameter optimization within OpenVSP, the user will be equipped with access to parametric design variables defined within the model.

VI. Conclusions

The overall objective of this effort was to demonstrate the feasibility of physics-based weight predictions for conventional and unconventional configurations. The feasibility and methodology of the approach were successfully demonstrated and results presented for a conventional (MD-87 commercial transport) and unconventional (Low Boom Flight Demonstrator) vehicle. The physics-based approach taken within the PBWeight software is capable of accurate weight and load response predictions for wing and fuselage designs, as well as capturing trends outside of historical databases. These initial results indicate a strong potential for making rapid and accurate weight predictions for unconventional designs.

Future work will include the refinement of the PBWeight software to further improve efficiency and applicability to a wide range of conventional and unconventional configurations. These refinements will also improve support for analyzing concepts with composite material properties and support for rapid weight and center-of-gravity predictions in parametric design trades. Other enhancements include the development and integration of a fully featured graphical user interface to the PBWeight tool within the OpenVSP parametric geometry modeling environment as well as automated wing-layout and fuselage-layout tools. Lastly, the refined PBWeight software will be verified and validated through demonstration on a range of configurations that are of interest to NASA and the broader technical community to ensure generality, robustness, and accuracy of the weight predictions.

Acknowledgments

Funding for the initial development of the PBWeight software was provided by NASA Langley, Phase I SBIR Project, Contract # NNX14CL76P. Ongoing development of the PBWeight software is provided by NASA Langley, Phase II SBIR Project, Contract # NNX15CL25C.

References

[1]Nicolai, L.M., and Carichner, G.E. *Fundamentals of Aircraft and Airship Design: Volume 1 - Aircraft Design,* American Institute of Aeronautics and Astronautics, Inc., Reston, VA, 2010.

[2]Raymer, D. P. *Aircraft Design: A Conceptual Approach,* American Institute of Aeronautics and Astronautics, Inc., 2012.

[3]Airport Compatibility Group, *MD-80 Series: Airplane Characteristics for Airport Planning,* Long Beach, CA : Douglas Aircraft Company, 1990.

[4]Ordaz, I., Geiselhart, K. A., and Fenbert, J. W. "Conceptual Design of Low-Boom Aircraft with Flight Trim Requirement," *32nd AIAA Applied Aerodynamics Conference,* AIAA, Atlanta, GA, 2014.

[5]M4 Engineering, Inc. *RapidFEM User Manaul Version 2.0.1,* Long Beach, CA : s.n., October 2012.

[6]Federal Aviation Administration, Hydraulic and Pneumatic Power Systems, *Federal Aviation Administration,* [Online] http://www.faa.gov/regulations_policies/handbooks_manuals/aircraft/amt_airframe_handbook/media/ama_ch12.pdf,

[7] Aircraft Familiarization DC-9, MD-80, MD-90, [Online]

[8]Boeing, How the Environmental Control System Works on Boeing Airplanes, *Boeing,* [Online] http://www.boeing.com/boeing/commercial/cabinair/environmentcontrol.page,

[9]PBS, Anatomy of a Jetliner, *NOVA*, [Online] PBS, February 2004. http://www.pbs.org/wgbh/nova/aircrash/jetl-nf.html. ,

[10]Federal Aviation Administration (FAA), *Metallic Materials Properties Development and Standardization (MMPDS)*, [Document] s.l. : Federal Aviation Administration (FAA), 2012.

[11]U.S. Government Publishing Office (GPO), TITLE 14 - Aeronautics and Space, *Electronic Code of Federal Regulations*, [Online] U.S. Government Publishing Office (GPO), December 16, 2014. http://www.ecfr.gov/cgi-bin/text-idx?tpl=/ecfrbrowse/Title14/14cfr25_main_02.tpl,